12-15-2014

# Characterization of Electrodeposited Copper Foil Surface Roughness for Accurate Conductor Power Loss Modeling

Michael B. Griesi
*University of South Carolina - Columbia*

# Characterization of Electrodeposited Copper Foil Surface Roughness for Accurate Conductor Power Loss Modeling

by

Michael B. Griesi

Bachelor of Science
University of South Carolina, 2013

---

Submitted in Partial Fulfillment of the Requirements

For the Degree of Master of Science in

Electrical Engineering

College of Engineering and Computing

University of South Carolina

2014

Accepted by:

Paul G. Huray, Director of Thesis

Olufemi B. Oluwafemi, Reader

Lacy Ford, Vice Provost and Dean of Graduate Studies

## DEDICATION

I dedicate this thesis to my wife Jessica. It was her love, support, understanding and patience that made this pursuit possible. I will be forever grateful.

## ACKNOWLEDGEMENTS

My deepest gratitude goes to my professor, advisor and committee chair Dr. Paul Huray. His passion for understanding the curious and nuanced intricacies of electromagnetic phenomenon is both inspiring and enlightening. It was through this passion I found a trusted mentor, leader and friend in our shared pursuit of understanding. Of particular importance to the completion of this thesis were Dr. Huray's integral research and development of the Huray surface roughness model accompanied by his detailed instruction provided throughout his lectures and publications.

A special thanks to my committee member Dr. Olufemi (Femi) Oluwafemi whose contributions to developing the snowball model provided practical relevance and legitimacy to the conclusions and impact of this thesis. Furthermore, his feedback was both motivating and constructive.

I especially want to thank John Fatcheric and Lee Lesher of Oak-Mitsui who contributed a significant amount of time explaining the process of manufacturing electrodeposited copper foil and providing a plant tour. Furthermore, they supplied most of the material and measurement tools for this research. The conclusions of this thesis are thanks to John and Lee's willingness to share their knowledge and resources.

I also want to thank Stephen Hall, who generously contributed constructive feedback for focused and practical content. As well, I would like to thank Christine Jones for graciously sharing additional VNA measurements and test board specifications that were critical for these conclusions. Thank you all.

## ABSTRACT

As computer data rates have increased, designers observed that the standard models for estimating the impact of copper foil surface roughness on conductor loss are limited to a few GHz. The more recent snowball model (a "snowball" estimation of the Huray Model) has demonstrated improved conductor loss predictions up to 50 GHz by estimating the necessary parameters using reasonable assumptions about the geometric surface features of electrodeposited copper foil. Since then, the Huray Model has been incorporated into commercial electromagnetic field simulators. However, a standard method of characterizing the electrodeposited copper foil used in high-speed circuits to directly implement the snowball model has not yet been fully established. Therefore, the primary objective of this thesis was to develop a method of more accurately characterizing the geometric parameters of electrodeposited copper foil surfaces for accurate conductor loss modeling as defined by the snowball model.

This thesis demonstrates the first methods of directly characterizing electrodeposited copper foil surface roughness to obtain snowball model parameters. Additionally, this research further legitimizes the analytic form of the snowball model as it pertains to scattered power, demonstrates the practical impact of its parameters, and reveals a source of existing irregularities between the estimated model parameters and actual performance measurements.

## PREFACE

This work is divided into six chapters. Chapter one introduces the motivation and reasons for this research. Chapter two reviews the history of conductor loss modeling, introduces electrodeposited copper foil and recent developments in conductor loss modeling. Chapter three meets the primary objective of this research by demonstrating methods for characterizing the surface of electrodeposited copper foil for accurate conductor loss modeling with results. Chapter four demonstrates a method for implementing the characterized parameters in commercially available simulation tools. Chapter five considers some limitations and concerns for the characterization methods described and alternatives measurements. Chapter six concludes with significant takeaways and recommendations for future work.

## TABLE OF CONTENTS

## LIST OF TABLES

## LIST OF FIGURES

## LIST OF SYMBOLS

| | |
|---|---|
| $A$ | Area (Square Meters) |
| $A_{flat}$ | Perfectly Flat Surface Area of Copper Foil (Square Meters) |
| $a_i$ | Radius of the $i^{th}$ Snowball (Meters) |
| $A_{matte}$ | Actual Untreated Surface Area of Copper Foil (Square Meters) |
| $\vec{B}$ | Magnetic Flux Density (Tesla) |
| $\delta$ | Skin Depth (Meters) |
| $\Delta$ | RMS Peak-to-Valley Surface Deviation (Meters) |
| $\vec{E}$ | Electric Field Intensity (Volts per Meter) |
| $\varepsilon_0$ | Permittivity of Free Space (Farads per Meter) |
| $\varepsilon_{r,2}$ | Permittivity of Propagating Medium (Dimensionless) |
| $\eta$ | Intrinsic Impedance of the Propagating Medium (Ohms) |
| $f$ | Frequency (Hertz) |
| $\vec{H}$ | Magnetic Field Intensity (Amperes per Meter) |
| $\vec{H}_0$ | Maximum Amplitude of Magnetic Field Intensity (Amperes per Meter) |
| $I$ | Electric Current (Amperes) |
| $\vec{J}$ | Electric Current Density (Amperes per Square Meter) |
| $k_2$ | Wave Number in the Propagating Medium (Meters) |
| $l$ | Length (Meters) |
| $\mu$ | Permeability (Henry per Meter) |

| | |
|---|---|
| $\mu_0$ | Permeability of Free Space (Henry per Meter) |
| $N_i$ | Total Number of Snowball of radial size $a_i$ (Dimensionless) |
| $P_{loss}$ | Electrical Power Loss (Watts) |
| $P_{rough}$ | Electrical Power Loss of a Rough Conductor (Watts) |
| $P_{smooth}$ | Electrical Power Loss a Smooth Conductor (Watts) |
| $R_{conductor}$ | Electrical Resistance (Ohms) |
| $\rho$ | Resistivity (Ohm Meters) |
| $\sigma$ | Conductivity (Siemens per Meter) |
| $\sigma_{absorbed}$ | Absorption Cross Section of Radial Size $a_i$ (Square Meters) |
| $\sigma_{scattered}$ | Scattered Cross Section of Radial Size $a_i$ (Square Meters) |
| $\sigma_{total}$ | Total Absorption and Scattered Cross Section (Square Meters) |
| $SR$ | Hall-Huray Surface Ratio (Dimensionless) |
| $\omega$ | Angular Frequency (Radians per Second) |

## LIST OF ABBREVIATIONS

CHT.....Circular Hough Transform

DC..... Direct Current

DSP .....Digital Signal Processing

ED .....Electrodeposited

FR-4 .....Flame Retardant 4

GHz .....Gigahertz

GI ..... Grade I

GIII.....Grade III

HFSS ..... High Frequency Structural Simulator

HTE.....High Temperature Elongation

kHz..... Kilohertz

MHT.....Mitsui High Temperature

MLS ..... Multi-Layer Shiny Side Treatment

PCB ..... Printed Circuit Board

PLSP ..... Plain Stain Proof

PTFE .....Polytetrafluoroethylene

RGB .....Red Green Blue

RMS .....Root Mean Square

SEM ..... Scanning Electron Microscope

TOB.....Treatment of Brass

VNA..... Vector Network Analyzer

# CHAPTER 1

## INTRODUCTION

With computer bus speeds increasing from only 108 kHz in 1971 to nearly 4 GHz in 2010 and even higher frequencies currently under development, the success of high-speed circuit designs depends more than ever on precisely predicting signal power loss [1] [2]. Interestingly, however, most of today's high speed bus designs rely on low-frequency circuit concepts with hypothetical parameters, rather than applying a first principle analysis to the propagation of high-frequency electromagnetic fields using properly characterized materials. In particular is the power loss prediction associated with copper foil conductors used in modern printed circuit boards (PCBs). While a low frequency analysis of conductor loss is rather simple, a high frequency analysis becomes especially challenging when considering the effects of a conductor's surface roughness geometry on electromagnetic fields.

The conventional method of estimating the impact of conductor surface roughness on electrical power loss is the Morgan-Hammerstad empirical fit. The conclusions of this empirical fit were based on a hypothetical surface roughness with illogical assumptions that contradicted causality and, in some instances, principles of relativity that has consequently proven incapable of suitably estimating conductor power losses above a few GHz. While there are a few modified forms of the Morgan-Hammerstad empirical fit which attempt to correct its inherent frequency limitation, they are all plagued by the same logic flaw that limits accurate conductor loss modeling to a relatively narrow band.

Recently, as industry struggled to increase bus speeds to 8 Gbps (4 GHz), the Huray surface roughness model was developed using a first principles analysis of high-frequency propagating electromagnetic fields in copper-based channels to enable logical and accurate conductor loss predictions for all frequencies. This provided a much needed fundamental description of conductor loss as determined directly from Maxwell's field equations. In order to provide industry with a simple and practical method of implementing the Huray surface roughness model, the snowball model was derived directly from the more general Huray surface roughness model to correspond with scanning electron microscope (SEM) images taken of electrodeposited copper foil used in modern high-speed transmission lines.

# CHAPTER 2

# BACKGROUND

## 2.1 ELECTRICAL CONDUCTOR LOSSES IN HIGH-SPEED TRANSMISSION LINES

At low frequencies, conductor losses are easily explained by Joule's first law:

$$P_{loss} = I^2 R_{conductor} \tag{1}$$

where $P_{loss}$ is the power lost to heat in W and $I$ is the current flowing through the conductor in amperes. $R_{conductor}$ is the resistance of the conductor in Ω defined as

$$R_{conductor} = \frac{\rho l}{A} \tag{2}$$

where $\rho$ is the resistivity in Ωm, $l$ is the length in m and $A$ is the cross sectional area in $m^2$. The simplicity of this analysis is thanks to a relatively uniform current density distributed throughout the entire thickness of a conductor at low, at or near DC, frequencies. However, as the frequency of the signal transmitted through the conductor increases, the exponentially decaying penetration depth, $e^{-x/\delta}$, of the current density reduces until it resides largely on the surface of the conductor effectively reducing the cross sectional area of the conductor and increasing the resistance as described by (2). This is well known as the skin effect and can be determined by

$$\delta(f) = \sqrt{\frac{2}{\omega\mu\sigma}} = \sqrt{\frac{1}{\pi f\mu\sigma}} \tag{3}$$

where $\delta$ is the exponential penetration depth of the current density in meters, $\omega$ is the angular frequency in rad/s of a propagating signal, $\mu$ is the permeability in H/m of the conductor, $\sigma$ is the conductivity in S/m of the conductor, and $f$ is the frequency in Hz of

a propagating signal. It is clear from (2) that the penetration depth decreases as frequency increases. It is important to note however, as the electric field intensity oscillates, so does the induced current density. In other words, the current is induced inside the conductor which penetrates up to an exponential depth (i.e. the skin depth) at the point of $e^{-x/\delta}$ magnetic field intensity and decays along with the electric field intensity as it oscillates 45° out of phase with the magnetic field intensity. This concept is critical when considering the distribution of current and the associated power losses in a practical conductor which has a rough surface rather than a flat surface. This would effectively isolate the current flow within the surface profile of the conductor as a function of frequency. The challenge is then to describe and predict how an irregular surface impacts conductor losses when the current density is not uniform and oscillates harmonically in time.

## 2.2 The Morgan-Hammerstad Empirical Fit

An early work that addressed the impact of surface roughness on conductor losses was written by Samuel Morgan and published in 1949 [3]. This research was inspired by existing measurements that observed conductor losses exceeded the predictions of (1) at 1 GHz and increased with higher frequencies, even after $R_{conductor}$ was calculated to account for a reduced skin depth. The approach was to analyze hypothetical transverse and parallel grooves in an imagined "rough" surface since there were no SEM instruments available in 1949. The study was simplified by choosing imagined rectangular and triangular grooves, and then extending them infinitely for a two-dimensional analysis rather than three since computers had not been developed in 1949 (Figure 2.1).

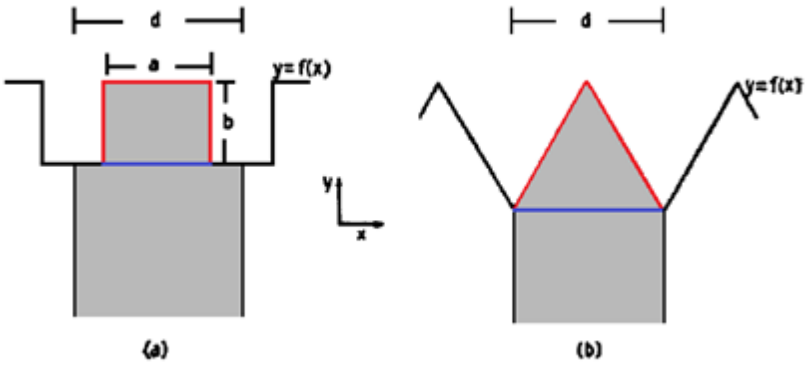


Figure 2.1 (a) Rectangular and (b) triangular surface grooves.

The red surface perimeter was varied to a maximum of twice the length of the blue path labeled *d* in Figure 2.1. Some later engineers have incorrectly interpreted this picture as if the electric field intensity propagating in the x direction in Figure 2.1 caused current traveling parallel to the grooved surface would need to travel along the longer red path of the transverse conductor grooves compared to a flat surface blue path. This concept led those engineers to conclude that increased conductor losses at microwave frequencies are caused by an increased current path length, effectively resulting in additional Joule heating for induced eddy currents. Morgan also analyzed electric field intensity in grooves parallel to the direction of propagation (i.e. the x direction) and concluded the power dissipation attributed to them was 36% of the impact attributed by transverse grooves.

In an effort to apply Morgan's work with a more practical calculation for high-speed copper channel designers, Erik Hammerstad presented an empirical fit to Morgan's transverse grooves as:

$$\frac{P_{rough}}{P_{smooth}} = 1 + \frac{2}{\pi} arctan\left[1.4\left(\frac{\Delta}{\delta}\right)^2\right] \quad (4)$$

where $\frac{P_{rough}}{P_{smooth}}$ is the ratio of power loss caused by a rough conductor versus a perfectly flat conductor, and $\Delta$ is the RMS deviation from a perfectly flat surface [4] [5]. This Morgan-Hammerstad empirical fit, which is only a mathematical guess to an accurate expression, attempts to describes the impact of a conductor's surface roughness as a function of eddy current flow with a relatively small skin depth at high frequencies isolated within the RMS deviation of the surface (Figure 2.2).

Figure 2.2 Current density isolated within the RMS surface roughness.

## 2.3 Problems with the Morgan-Hammerstad Empirical Fit

There is no scientific basis for the $arctan$ function in (4); it is simply a **guess** of a function that empirically fits Morgan's two-dimensional data. This function's asymptotic maximum of 2.00 roughly agrees with Morgan's results since Morgan chose a maximum increased path length (i.e. the red perimeter in Figure 2.1) of 2.00. In practice however, the surface roughness can impact power loss greater than a factor of 2.00. Also, (4) does not consider power loss which may be contributed by parallel grooves. Although Morgan considered the impact of parallel grooves to be 36%, Hammerstad chose to ignore it. Using Hammerstad's empirical fit, high-speed bus designers have been able to predict conductor losses within practical error up to about 4 GHz. However, these predictions were observed to break down as bus speeds approached 8 Gbps [6]. Specifically, performance measurements indicated conductor losses were greater than predicted when

using the empirical fit, implying that the fit tends to underestimate these losses with a growing error trend for all frequencies greater than a few GHz (Figure 2.3) [7].

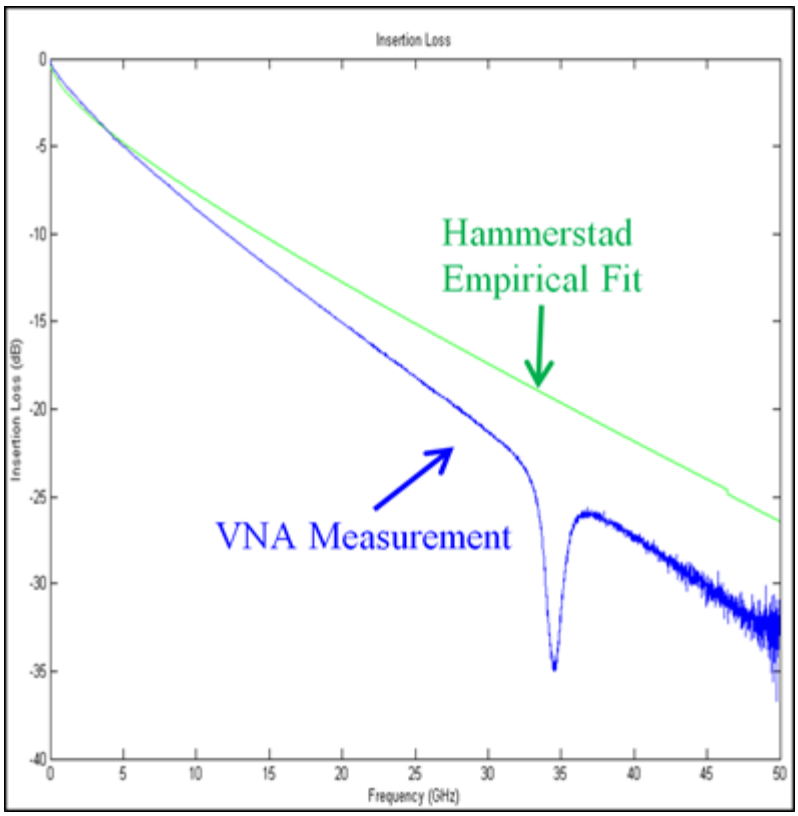


Figure 2.3 Hammerstad Fit vs. VNA measurement of 7" microstrip.

Any simple modification to (4) will not adequately solve this logical problem because there is a fundamental flaw in the premise behind the empirical fit. Morgan's two-dimensional transverse grooves assume the skin depth follows the surface profile (i.e. skin depth is normal to the surface at any point), causing the current to travel a farther distance. While it is true that a reduced cross section and increased length would increase Joule heating (1-2), it cannot be true that the current density follows the surface profile (Figure 2.4).

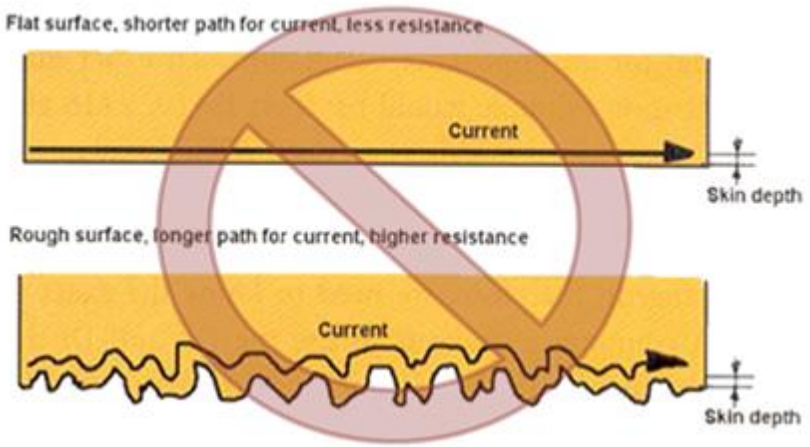


Figure 2.4 Incorrect current path for a rough surface with skin depth. [8]

In order for Figure 2.4 to be true, 1 of these 2 observations must be true:

1. Propagation delay between a transmitter and receiver increases.
2. Causality and in some instances principles of relativity are violated.

Since the propagation delay between a transmitter and receiver does not increase as a function of surface roughness, we are left with the contradictions to causality and relativity. It is important to remember that the surface current density is induced by Gauss's Law applied to a propagating electric field intensity in the horizontal direction. To begin with causality alone, there is no mechanism for surface current density to reverse when it encounters a hook like structure without the field reversing. Likewise, current density cannot instantaneously flow vertically when it encounters a vertical structure without the field somehow pausing, which would then violate Faraday's law even if it were possible. Relativity can be discussed with a single substrate media such as FR-4 where a propagating electric field is traveling a 1/2 the speed of light. Then when reconsidering Morgan's equilateral triangular surface, the propagating electric charge density would need to travel at the speed of light since the distance traveled would be

doubled, as illustrated in Figure 2.1. Worse off, as the permittivity of the media decreases (e.g. Teflon ≈ 2.08) or the surface roughness increases beyond 2.00, charge density would need to travel **faster** than the speed of light. Since neither of the conditions necessary to support Figure 2.4 is met, it is clear that the Hammerstad empirical fit is not a physical model of surface roughness but rather a convenient rule of thumb that works for some frequencies. It is not surprising then that the empirical fit tends to break down at some frequency, which happens to be around 4-5 GHz for a microstrip transmission line. While there has been value in the empirical fit for designers, higher frequency designs need to consider a first principles method for modeling conductor losses.

In order to calibrate our understanding of current density in a high-speed circuit, the current density should be thought of as eddy currents induced by a surface charge density that's caused by a propagating signal electric field intensity displacing electrons, transverse to the surface, rather than a discrete current traveling along the surface path as shown in Figure 2.4. This idea is a bit more intuitive when considering an isolated conducting feature near the conductor but not in contact (Figure 2.5).

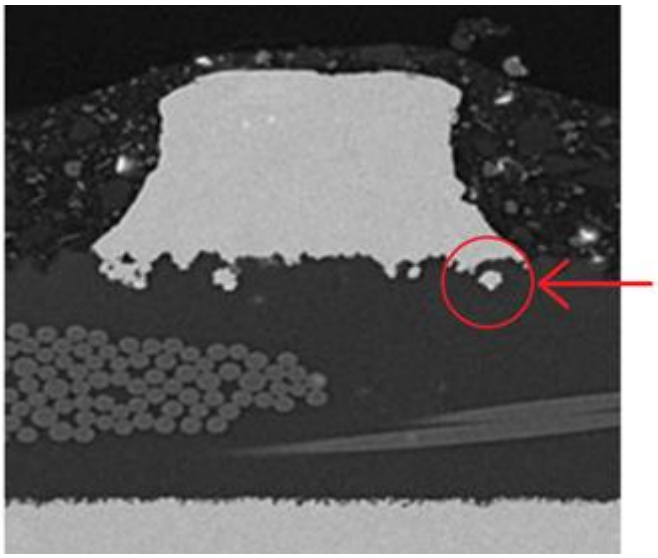

Figure 2.5 Cross sectional view of isolated copper below a microstrip.

If current were to flow discretely through the conductor, there would be no way for current to also travel through an isolated feature. It is quite clear that any current residing in this feature would be induced eddy currents. Likewise, the power loss caused by the surface roughness can be thought of the same way as the isolated feature. Since eddy currents are directly proportional to the frequency

$$\sigma\nabla \times \vec{E} = -\nabla \times \vec{J} = -j\omega\mu\sigma\vec{H} \tag{5}$$

(marginally simplified by assuming a large conductivity), where $\vec{E}$ is the electric field intensity in volts/m, $\vec{J}$ is the electric current density in amperes/m$^2$, and $\vec{H}$ is the magnetic field intensity in. amperes/m, an increase in eddy currents induced over an increased surface area at high frequencies would result in higher losses, rather than increased resistance over length (Figure 2.6).

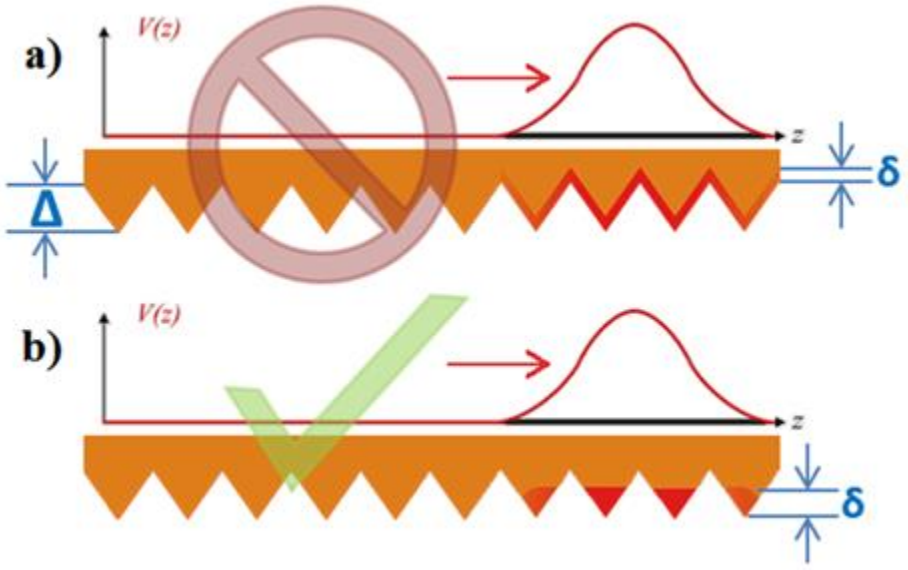


Figure 2.6 (a) Traditional vs (b) fundamental current density in high-speed conductors.

The integral form of Faraday's equation highlights the double integration of the magnetic flux density $\vec{B}$ over a surface area

$$\oint_c \vec{E} \cdot dl = -\frac{d}{dt} \iint_s \vec{B} \cdot dS \tag{6}$$

as opposed to the single length dimension used in the empirical fit. This idea changes our traditional view of ohmic losses as determined by RMS surface deviation and skin depth to a fundamentals based view of electromagnetic field losses based on electric field intensity and induced surface charge density as determined by the total surface area. It is the absorption and scattering of these fields from the increased surface area of these irregular features which contribute to conductor losses at high frequencies. For that reason, the geometric features of the conductor surfaces used in high-speed PCB design need to be carefully examined and characterized for accurate conductor power loss modeling.

## 2.4 Electrodeposited Copper Foil

As concluded in Section 2.3, it is necessary to examine the surfaces of the conductors used in high-speed PCB design. This is almost always a form of electrodeposited (ED) copper foil for its dimensional consistency, peel strength, and electrical characteristics. Today's manufacturer's use 3 main phases to fabricate these foils (Figure 2.7).

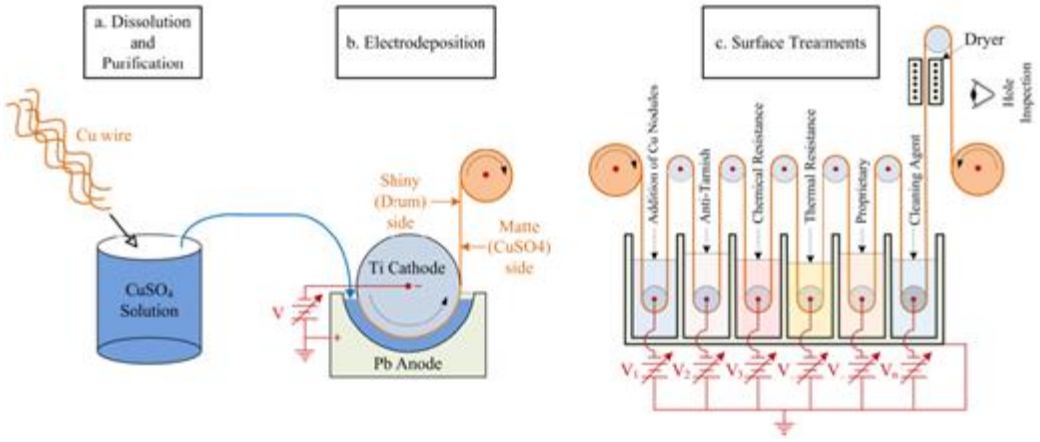


Figure 2.7 Three phases of ED copper foil fabrication. [9]

The electrodeposition and surface treatment phases (b and c in Figure 2.7) play key roles in determining the surface roughness of the ED foil. To begin, there are 2 sides of the foil made during the electrodeposition phase; the "drum side" and the "matte side". The surface roughness of the drum side (also known as the "shiny side" in Figure 2.7 b) is determined by the roughness of the drum, or titanium cathode, itself. These drums are polished to have an extremely smooth surface which creates the "low profile" side of the ED foil with an average deviation in the z-axis height as low as 0.3 μm (Figure 2.8).

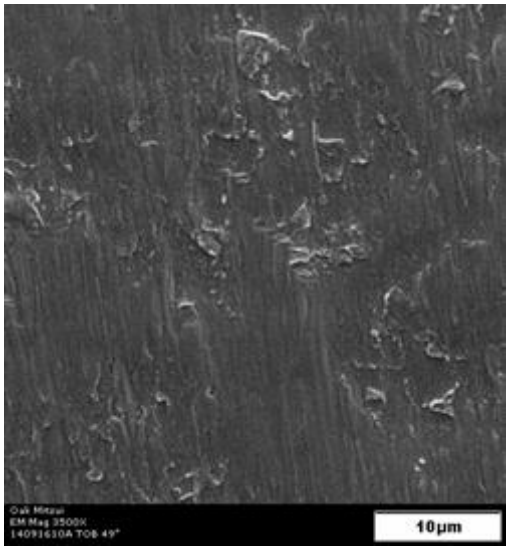


Figure 2.8 Oak-Mitsui Untreated Drum Side 0.5 oz MLS GIII HTE foil 3500x.

The surface roughness of the matte side is determined by how uniformly the copper grows outward from the drum. Several factors contribute to this surface such as the flatness of the base (i.e. the drum), the purity of the copper sulfate ($CuSO_4$), the uniformity of the electric field, the pH and temperature of the solution, and the time allowed for growth as determined by the electrodeposition over potential and current. Since so many factors are associated with determining surface of the matte or "high

profile" side of the ED foil, it usually has a larger deviation in the z-axis height typically ranging from 2-25 μm (Figure 2.9).

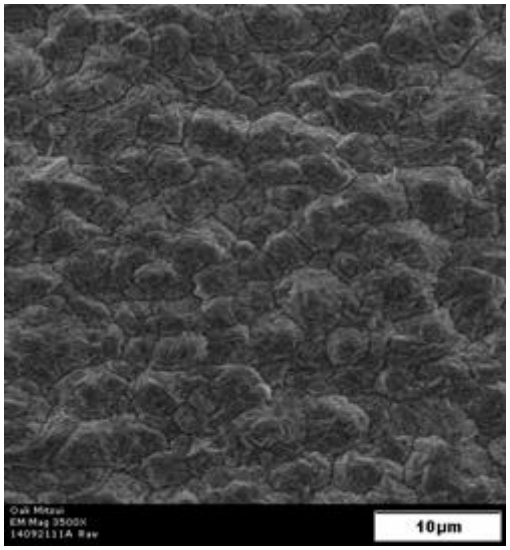


Figure 2.9 Oak-Mitsui Untreated Matte Side 0.5 oz TOB GIII HTE 3500x.

After the electrodeposition phase, a number of surface treatments are given to the foil for mostly mechanical and chemical properties such as anti-tarnish, chemical resistance, thermal resistance, and PCB adhesion. Of particular interest to the electrical properties are the copper dendrites or "anchor nodules" grown on the surface for PCB adhesion. These anchor nodules leave pockets for resin to fill during PCB lamination to increase the mechanical adhesion, referred to by its test name "peel strength". The size and distribution of anchor nodules may be affected by the surface profile fabricated during the electrodeposition phase. While manufacturers typically have a substantial degree of control over this, there are generally 2 different distribution arrangements of anchor nodule growth; one for the drum side and another for the matte side. The anchor nodules on the drum side appear similar in size and distributed uniformly across the surface (Figure 2.10).

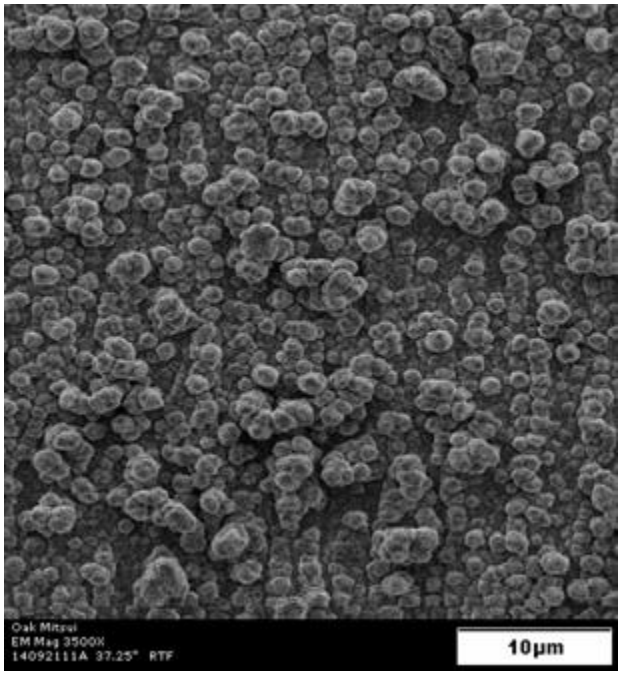


Figure 2.10 Oak-Mitsui Treated Drum Side 0.5 oz MLS GIII HTE foil 3500x.

The anchor nodules on the matte side, however, appear to concentrate towards the peaks of the untreated matte surface (Figure 2.11).

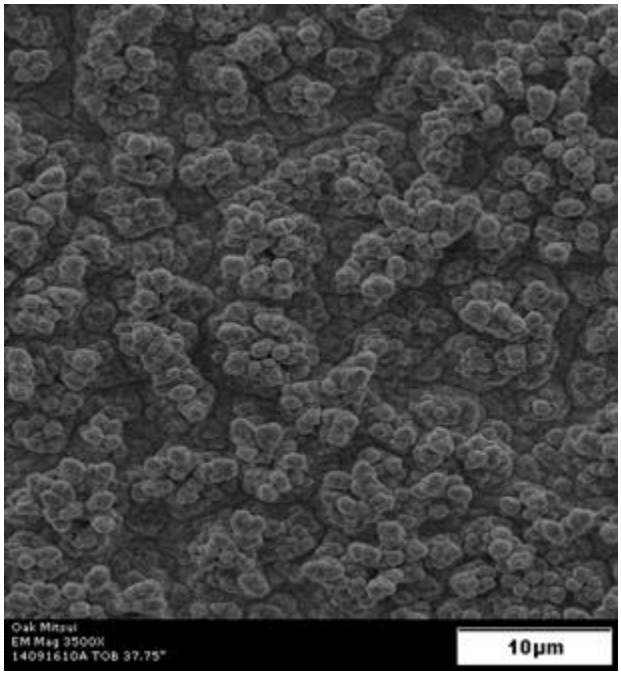


Figure 2.11 Oak-Mitsui Treated Matte Side 0.5 oz TOB GIII HTE 3500x.

Therefore, in order to examine and characterize the surface as concluded in Section 2.3, two components must be analyzed. The first is the surface area of the untreated ED foil before anchor nodules are deposited. The second is the surface area of the anchor nodules themselves. Both analyses are necessary for accurate conductor power loss modeling.

## 2.5 The Snowball Model

In an effort to describe the impact in terms of the untreated ED foil and the geometric features of any surface anomalies such as anchor nodules as concluded in Section 2.4, Dr. Paul Huray applied a first principles analysis to describe the power loss of a conductor's rough surface with respect to a flat surface

$$\frac{P_{rough}}{P_{smooth}} \approx \left[\frac{\mu_0 \omega \delta}{4}|H_0|^2 A_{Matte} + \sum_{i=1}^{j} N_i \sigma_{total,i} \frac{\eta}{2}|H_0|^2\right] \Big/ \left[\frac{\mu_0 \omega \delta}{4}|H_0|^2 A_{Flat}\right] \qquad (7)$$

where $H_0$ is the local magnetic field intensity maximum in amperes/m, $A_{Matte}$ is the untreated copper foil surface area (drum side or matte side) without anchor nodules $m^2$, $A_{Flat}$ is the perfectly flat two-dimensional area in $m^2$, $\mu_0$ is the permeability of free space in H/m, $N_i$ is the total number of surface spherical features of radial size $a_i$ , $\sigma_{total,i}$ is the total absorption and scattering cross sections of radial size $a_i$ spheres in $m^2$, and $\eta$ is the intrinsic impedance of the propagating medium in Ω. Taking a closer look at the anchor nodules reveals a stack-up of copper balls which resemble "snowballs" (Figure 2.12).

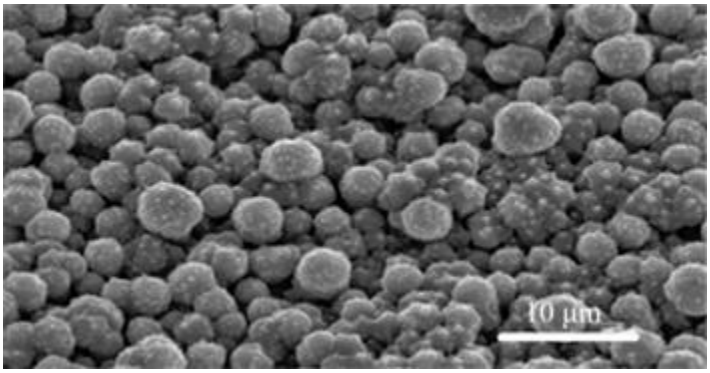


Figure 2.12 Gould Treated Drum Side 5000x.

Approximating the snowballs to spheres and substituting the cross section of a distribution of *j* different sized snowballs into (7) yields

$$\frac{P_{rough}}{P_{smooth}} \approx \frac{A_{Matte}}{A_{Flat}} + 6\sum_{i=1}^{j}\left[\left(\frac{N_i \pi a_i^2}{A_{Flat}}\right)\Big/\left(1+\frac{\delta}{a_i}+\frac{\delta^2}{2a_i^2}\right)\right] \quad (8)$$

where $a_i$ is the radius of the $i^{th}$ snowball (sphere). In this equation, two assumptions have been made: the absorbed power is so much larger than scattered power that the latter may be neglected and that the dipole terms in the absorption are so much larger than the quadrupole (and higher) terms that the latter may be neglected. The form of (8) clearly isolates the two components concluded in Section 2.4, where $\frac{A_{Matte}}{A_{Flat}}$ describes the ratio of surface area of the untreated ED foil before anchor nodules are deposited to a perfectly flat surface area and the remainder describes the total surface area of the various sized snowballs per unit flat area in the (parenthesis of the numerator) modified by the frequency dependence in the (parenthesis of the denominator). Furthermore, the form of (8) allows for a simple analysis of (7) requiring the surface characterization of only three measurable components (Table 2.1).

Table 2.1 Conductor Surface Parameters of the Snowball Model

| Parameter | Description |
|---|---|
| $A_{Matte}/A_{Flat}$ | The relative surface area without snowballs per unit flat area |
| $a_i$ | The radius of the $i^{th}$ snowball |
| $N_i/A_{Flat}$ | The number of snowballs with radius $a_i$ per unit flat area |

Channel performance VNA measurements have been used to fit estimations for the 3 parameters of (8) which have demonstrated improved channel loss prediction within

industry and have subsequently been incorporated into commercial electromagnetic field simulators. The qualitative accuracy of the snowball model in dB/in was determined to be within 1% of measured transmission line losses up to 50 GHz using these estimations for a 7" microstrip (Figure 2.13). While a qualitative verification has only been performed up to 50 GHz, the snowball model is predicted to maintain the same accuracy up to a minimum of 100 GHz.

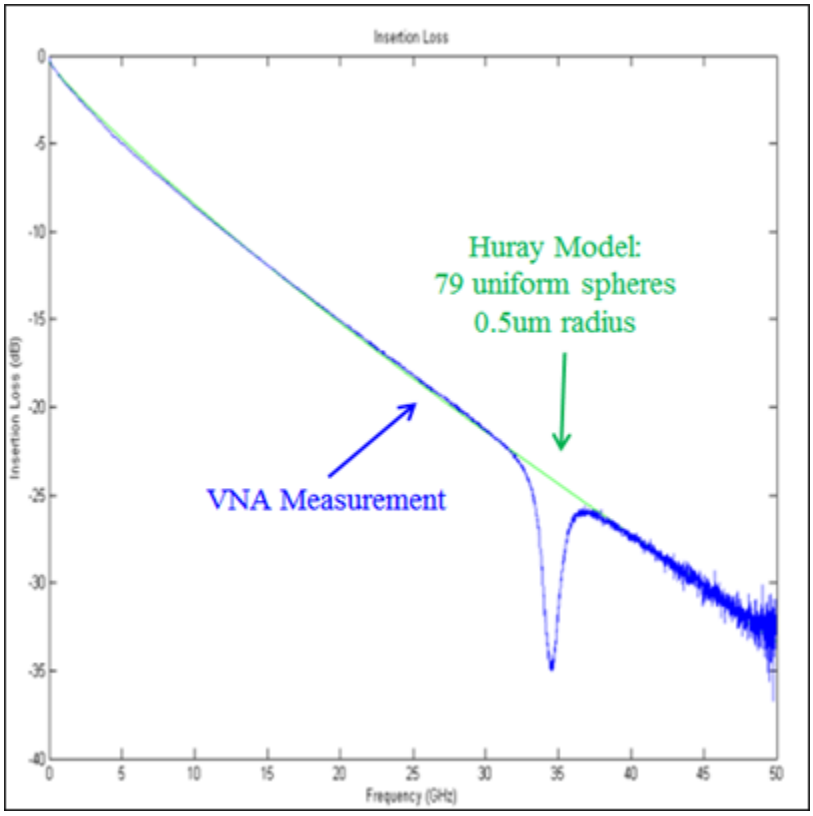


Figure 2.13 Snowball model vs. VNA measurement of 7" microstrip.

## 2.6 Objections to and Problems with the Snowball Model

The first and perhaps most pressing question about the first principles snowball model is whether it is necessary. The Hammerstad empirical fit to Morgan's two-dimensional data has served bus designers for more than 30 years with acceptable error

up to about 4-5 GHz, depending on the length of the transmission line. From an academic perspective, the Hammerstad empirical fit exploits our mistaken intuition for eddy current paths in high-speed conductors, ignores our conviction in causality, and challenges our fundamental understanding of relativity; as evident from Figures 2.4 and 2.6. Conversely, the snowball model clears this misunderstanding by providing a description which agrees with the standard model of propagating electromagnetic fields in a dielectric (like FR-4) at a boundary with a good conductor (like copper). Without this clarification, scientific and technological advances are easily hindered by misidentifying the root cause of electromagnetic power absorption caused by conductor surface roughness.

This leads to the impact it has on industry when designing higher-speed digital communications using copper channels. To begin, copper channels are plagued with inherently low-pass filter characteristics, which limits trace length to account for signal loss and distortion at high frequencies. Even at lengths as short as 1 inch, the impact of ED foil surface roughness on signal power absorption becomes significant at frequencies above 1 GHz. Although it may be true that the empirical fit has performed well in the past up to a few GHz, Figure 2.3 clearly illustrates its practical limitations. In fact, the loss error in dB/in associated with the empirical fit continues to grow after only a few more GHz, resulting in unacceptably large errors. When comparing the predictions of the snowball model in Figure 2.13 to the predictions of the empirical fit in Figure 2.3, it becomes quite clear that high-speed designs which exceed 5 GHz will require a new model to prevent significantly underestimating signal loss, which can be provided by the snowball model. Underestimating this loss would most certainly lead to unanticipated closed signal “eyes” at the receiver and ultimately inhibit operational success of the

design. In short, future designs at frequencies above a few GHz will need to consider an improved method of predicting conductor loss. The snowball model can fulfill that need for industry designs of the near future. At a minimum, the snowball model can allow designers to accurately predict these losses and design around them. The snowball model provides a clear root cause that future designs can use to mitigate the effects of surface roughness; which is not possible with the empirical fit since the Hammerstad fit is incorrect.

Another concern about the snowball model is revealed with a closer look at the derivation of (8) from (7). When a propagating signal encounters a good conducting sphere, like an approximation for a copper snowball, the signal can either be scattered (outgoing power) or absorbed (incoming power). The total cross section for a copper snowball is then the sum of the absorption and scattering cross sections

$$\sigma_{total} = \sigma_{absorbed} + \sigma_{scattered} \tag{9}$$

If the absorption and scattering cross sections (neglecting quadrupole and higher multi-pole terms) are deduced as

$$\sigma_{absorbed}(\omega) \approx 3\pi k_2 a_i^2 \delta \Big/ \left[1 + \frac{\delta}{a_i} + \frac{\delta^2}{2a_i^2}\right] \tag{10}$$

and

$$\sigma_{scattered}(\omega) \approx \frac{10\pi}{3} k_2^4 a_i^6 \left[1 + \frac{2}{5}\left(\frac{\delta}{a_i}\right)\right] \tag{11}$$

where the wave vector for the non-conducting medium is

$$k_2 = \omega\sqrt{\mu_o \varepsilon_o \varepsilon_{r,2}} \tag{12}$$

and the intrinsic impedance of the propagating medium is

$$\eta = \sqrt{\mu_o / \varepsilon_o \varepsilon_{r,2}} \tag{13}$$

then (8) disregards the scattered cross section. While (7) is entirely capable of considering the effects of scattered power, the calculations become arduous. With this in mind, we can ask: "To what extent can the scattered cross section be ignored?" That is, to determine at what frequencies are the effect of scattered power negligible. By normalizing (10) and (11) to the geometric cross section of an individual snowball of size *i*, their effects can be compared directly as a function of frequency (Figure 2.14).

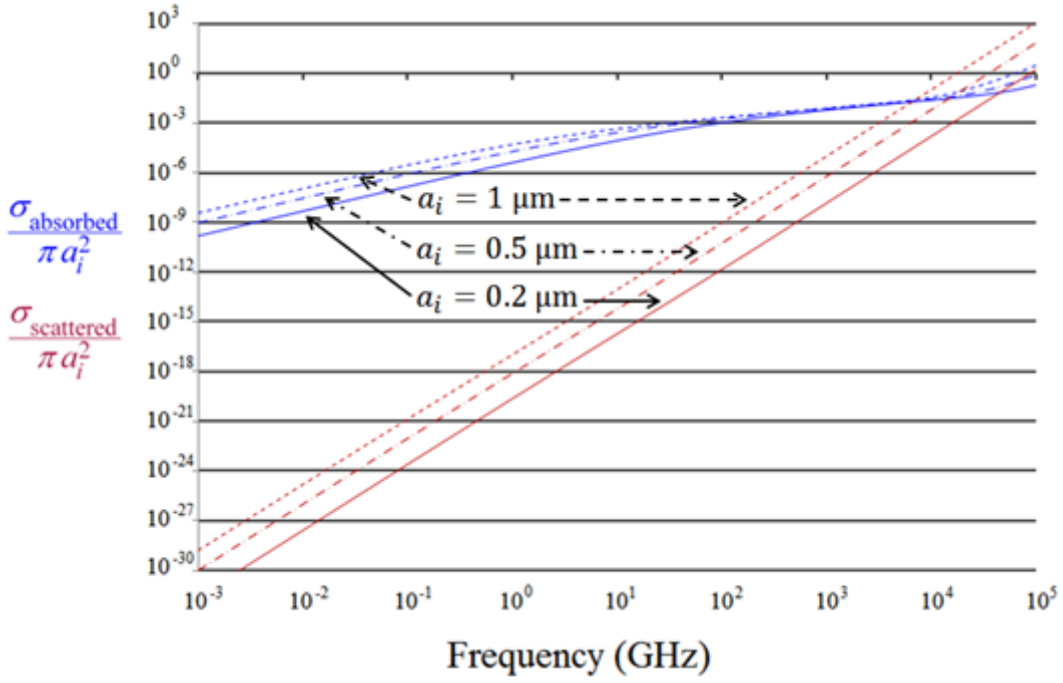


Figure 2.14 Absorption and scattering cross-sections of various size copper spheres. [10]

Selecting a reasonable radial length of $a_i = 0.5$ µm at 100 GHz, we can see that the scattered cross section is only $10^{-11}$ of the geometric cross section, which is also relatively minute when compared to the absorbed cross section at $10^{-3}$. As well, the scattered cross section reduces at a rate of about $10^{-4}$ per decade of frequency. So, if a 36% impact has been considered 'negligible' by the Hammerstad empirical fit for the past 30 years, it seems sensible to consider a $10^{-9}$ impact or less as negligible in this approximation.

Therefore, the practical answer to when the scattered cross section can be ignored is: for all frequencies below 100 GHz. Only when frequencies are above 100 GHz, and certainly as they extend into the optical range (i.e. above 10 THz), will the effects of scattered power have a significant impact. Thus, by accepting an error of $10^{-9}$ to be negligible, (8) is justified in disregarding the scattered cross section.

A problem with the snowball model as it exists today is that industry has had trouble in obtaining the 3 necessary parameters listed in Table 2.1. So far, performance correlation has been made by measuring a channel after fabrication and fitting the parameters to match the measured data. For each of these parameters, assumptions were made about the surface of the ED foil to estimate their values. The assumptions were:

1. Snowball stack-ups can be treated as uniform, average sized spheres.
2. The number of snowballs can be ascertained using a perfectly flat base.
3. The surface (without snowballs) is flat (i.e. $A_{Matte}/A_{Flat} = 1$).

Using SEM images, each of these assumptions can be investigated. The first assumption simplified $a_i$ by assuming all snowballs were the same size and assigning a single value. However, real snowballs have many different sizes (Figure 2.15).

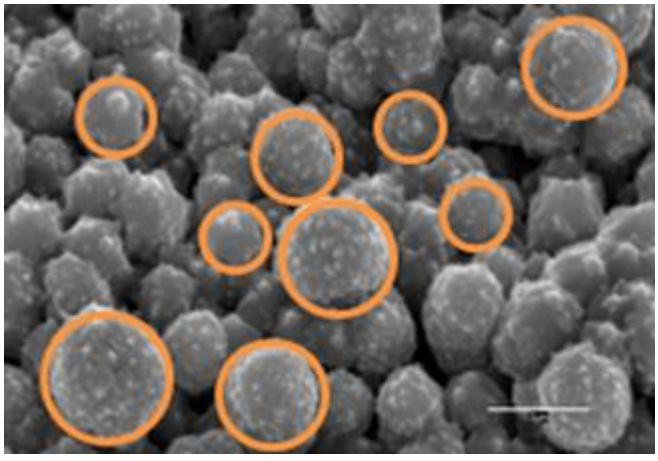

Figure 2.15 Distribution of snowball sizes emphasized with orange rings.

The second assumption simplified $N_i/A_{flat}$ by assuming the base of the stack-up was flat. However, a close look at the surface before snowballs are added, reveals that the base is not perfectly flat (Figures 2.8 and 2.9). This could alter the number of snowballs in a stack up as compared to the estimated number of snowballs in a stack up by reducing the available volume (Figure 2.16).

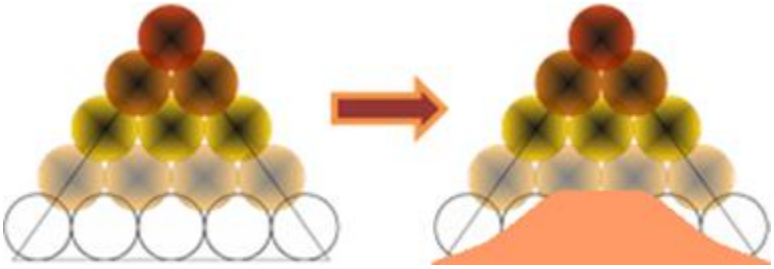

Figure 2.16 Altered number of snowballs in stack-up caused by an irregular base.

Furthermore, the number of snowballs per unit area may change between products since the distribution of snowballs change with different bases (drum side or matte side) as described in Section 2.4 (Figure 2.17).

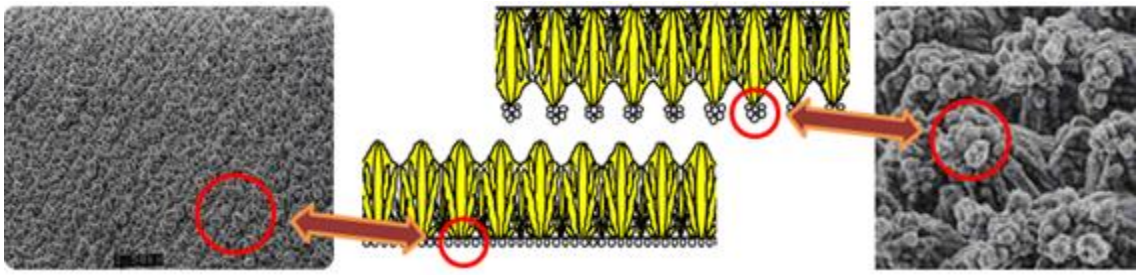

Figure 2.17 Snowball densities on drum side (left) vs. matte side (right).

The third assumption simplified $A_{matte}/A_{flat}$ by assuming it was flat in order to estimate the number of snowballs in the second assumption.

While these assumptions have demonstrated the model's usefulness and potential accuracy to within 1% from 5-50 GHz for channels up to 7", they still exhibit minor deviations between approximations in the snowball theory and measurement as a function of frequency. It is the primary objective of this thesis to address this problem by describing and demonstrating a method of more accurately characterizing the surface of electrodeposited copper foil in order to obtain the 3 parameters for industry implementation.

# CHAPTER 3

# COPPER FOIL SURFACE CHARACTERIZATION

## 3.1 IMPACT OF SNOWBALL MODEL PARAMETERS ON CONDUCTOR LOSS

Much of the text and images in this chapter have been submitted for a technical conference paper and presentation [22]. Before considering practical methods of characterizing copper foil to obtain parameters for the snowball model, it is important to determine if a snowball radii distribution is necessary or whether a single average radius is sufficient. This was assessed by calculating (8) for skewed, narrow and wide distributions, and a single average radius for comparison, all with the same total number of snowballs per unit flat area. The Morgan-Hammerstad empirical fit (4) was also calculated for comparison. The small and large skewed distributions did not reveal any surprises. It was expected that a decrease in surface area would result in a decrease in power loss and vice versa. What's particularly interesting is how a normal distribution of snowballs with the same average size as the single average results in a significantly different magnitude and slightly shifted point of inflection. Results show that as the standard deviation of a normal distribution of snowball radii increases, the power loss also increases, even though the average size of the snowballs remains constant (Figure 3.1). If instead, the **volume** of added copper in the nodules is the same for all radii, then the surface area of small radii per unit volume will be much larger for small spheres as for large spheres. Therefore, each of the 3 parameters defined by the snowball model play a distinct role in

predicting conductor losses over a wideband, and should be determined completely and independently for the most accurate results.

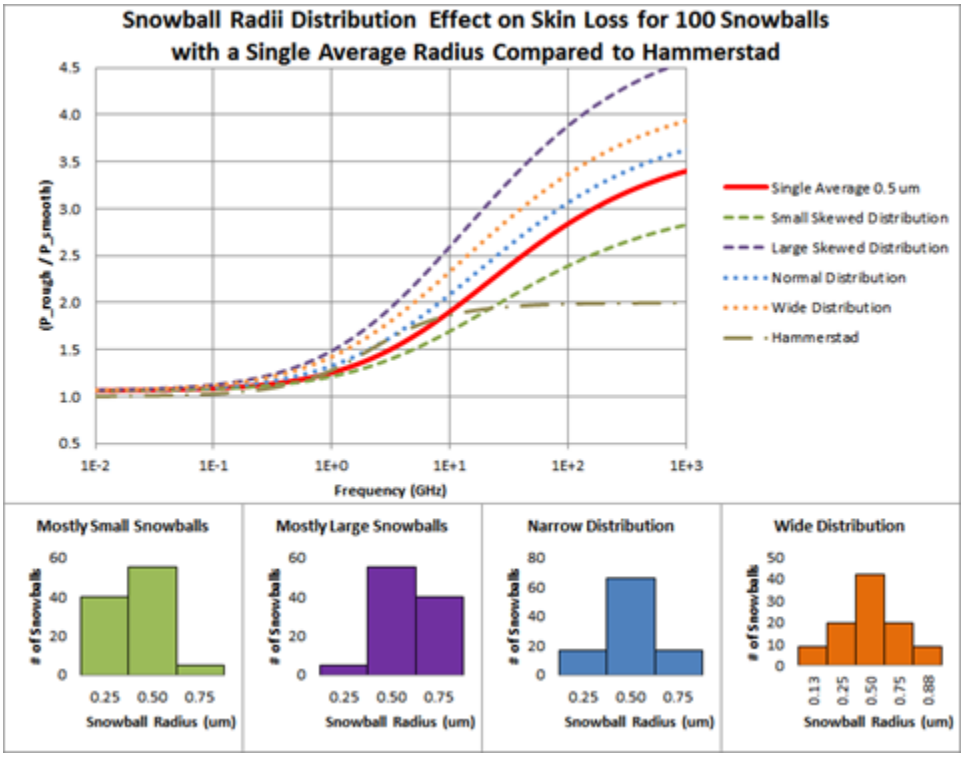


Figure 3.1 Distribution effect on skin loss.

The impact of snowball distributions on power loss is shown in Figure 3.2.

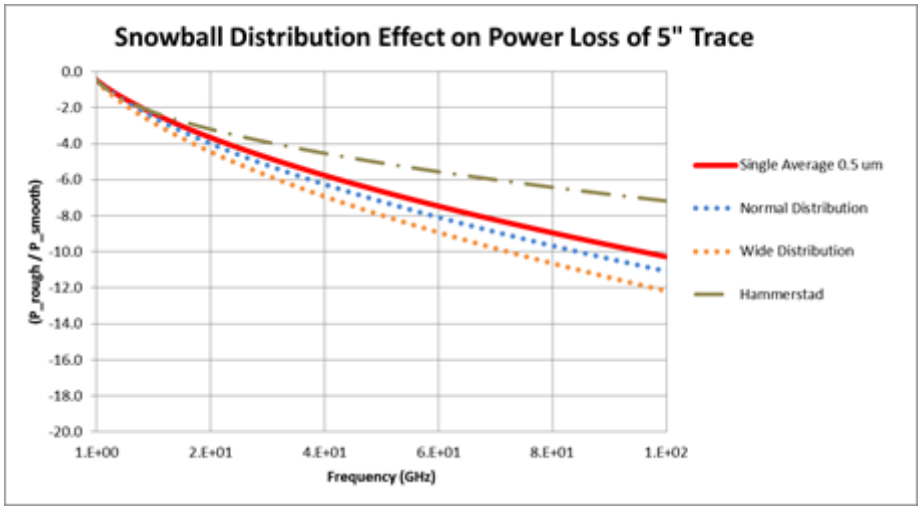


Figure 3.2 Distribution effect on power loss for a 5" microstrip.

Although Figure 3.1 demonstrates the impact of a distribution of snowball radii, it does not clearly demonstrate the impact of a *uniform* radius. That is, a single radius for all $N_i$ that is not necessarily the average radius. This was assessed by comparing the narrow and wide distributions to a single uniform radius with an impact of similar magnitude (Figures 3.3 and 3.4).

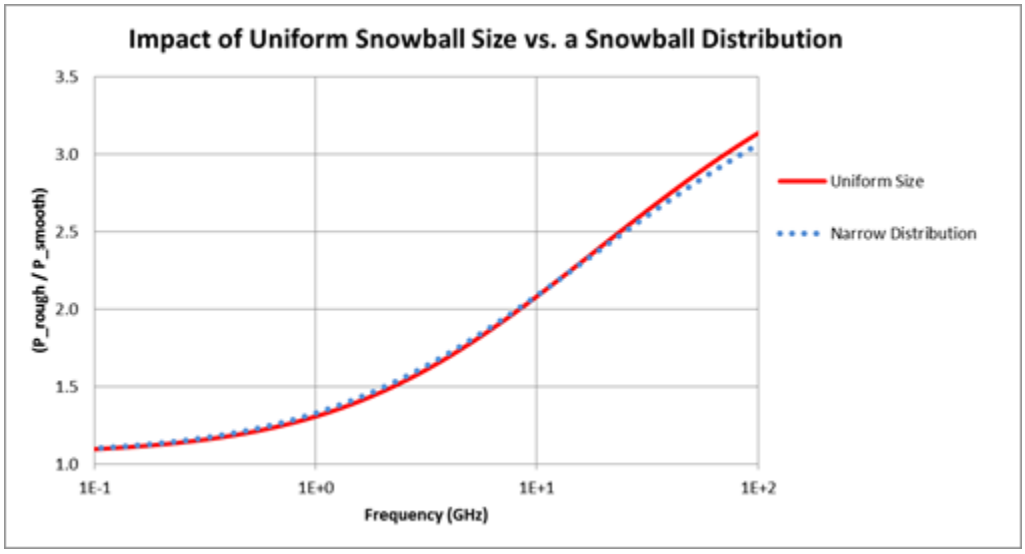


Figure 3.3 Effect of a uniform snowball radius vs. a narrow distribution of radii.

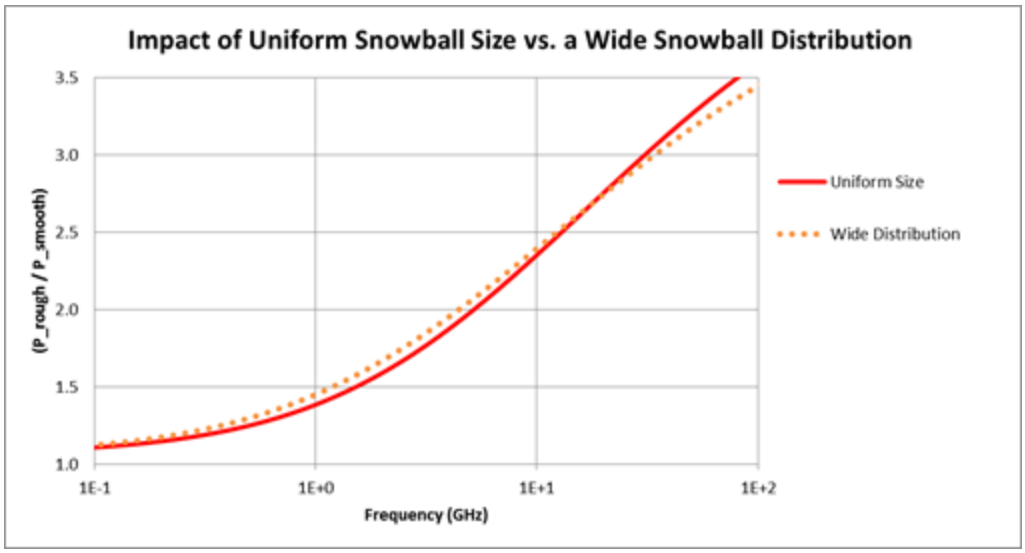


Figure 3.4 Effect of a uniform snowball radius vs. a wide distribution of radii.

Figures 3.3 and 3.4 demonstrate the impact of a distribution of snowball radii as described by Figure 2.14. This low-to-high frequency inflection point suggests an increased impact on conductor loss at relatively low frequencies and a slightly reduced impact at higher frequencies which is also proportional to the standard deviation of the snowball radial length distribution. This data could provide an explanation for the error observed in [7] when correlating the snowball model with VNA measurements.

Another concern of interest is that any characterization performed before PCB lamination might not predict the impact of snowballs shifting during the annealing process. This is not expected to have any significant impact since (8) is not dependent on where the snowballs are located and there is no reason to believe a shift in location would alter the average snowball density $N_i/A_{Flat}$ for the total area.

## 3.2 Characterizing Treated Copper Foil: $a_i$ and $N_i/A_{flat}$

In order to obtain $a_i$ and $N_i/A_{flat}$, images must be taken of the treated copper surface with enough magnification and resolution to easily distinguish the snowballs while maintaining the largest field of view possible. A nice balance was found for these criteria at a magnification of 3500x. There are 2 methods presented for obtaining a snowball distribution. The first method uses images taken by an SEM, and the second uses images taken by a 3D digital microscope. After the images are obtained, there are 3 challenges to extracting $a_i$ and $N_i/A_{flat}$:

1. Identify all of the snowballs in the image.
2. Count the number of snowballs in the image.
3. Measure the radius of each snowball in the image.

Performing these 3 challenges manually would not be a practical solution. Some common approaches to automating image feature detection include binarization and RGB thresholding to isolate the foreground from the background, usually after clustering and filtering [11] [12] [13]. However, it was found that these methods did not prove reliable for this type of analysis since they often missed snowballs in the filtered background and clumped neighboring snowballs together in the foreground. Since the snowballs are approximately spherical, and thus circular in a 2D image, a more appropriate choice is a Circular Hough Transform (CHT) [14]. While a CHT can identify partially hidden snowballs, one possible drawback to analyzing a 2D image of the surface is that there may be snowballs completely hidden beneath other snowballs. This may be a concern if the surface had several layers of snowballs. If this is a concern, it may be possible to analyze a cross-section of the foil to determine how many layers of snowballs are stacked and extend the surface distribution to the appropriate number of layers, but this was not performed during this research.

### 3.2.1 SEM Analysis Method

The SEM used to capture images of the treated copper foil was an SEII v2.3 PCI SEM (Figure 3.5).

Figure 3.5 SEII v2.3 PCI Scanning Electron Microscope (SEM).

The previously recommended magnification of 3500x was chosen since it gave the largest field of view where the snowballs were still readily visible. Five samples were analyzed from 5 positions across the entire width of two rolls of copper foil, 1 treated drum side and 1 treated matte side, illustrated in Figures 2.10 and 2.11 respectively. After SEM images were captured, MATLAB was used to implement a CHT and identify the snowballs (Figure 3.6).

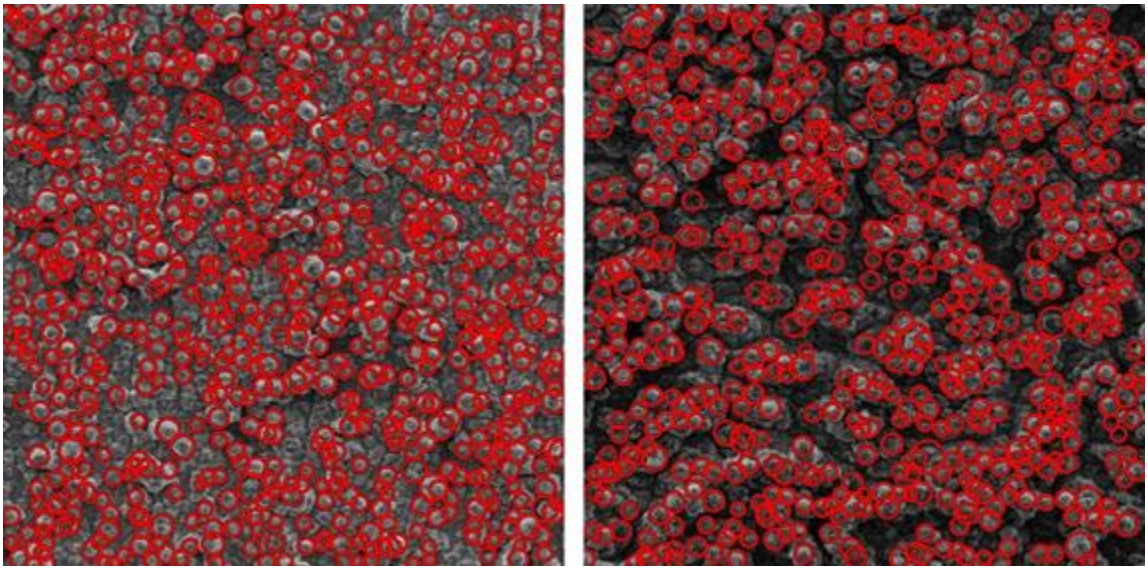

Figure 3.6 MATLAB Snowballs on Drum (left) and Matte (right) Sides.

Although the CHT algorithm in MATLAB is quite simple, some initial care should be taken to fine tune the sensitivity and edge detection threshold for the first image to qualitatively assess whether too many or too few snowballs are being detected. After these are set initially, all subsequent analyses should be standardized to the same settings. After the snowballs are identified, MATLAB can also be used to count the number of snowballs and measure their respective radii (Figure 3.7).

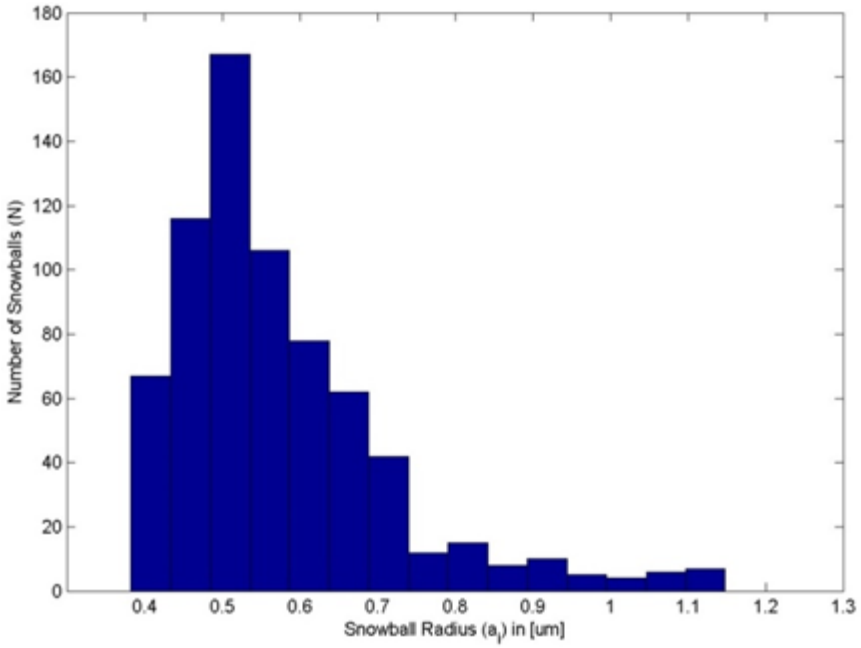


Figure 3.7 Snowball Radii Distribution of Drum Side from SEM Method.

Distributions were divided into 15 bins. Drum side analysis determined an average $a_i$ of 0.54 μm with a standard deviation of only 0.03 μm and an average $N_i/A_{flat}$ of 45 snowballs per 100 μm$^2$ with a standard deviation less than 3 snowballs per 100 μm$^2$. Matte side analysis determined an average $a_i$ of 0.56 μm with a standard deviation of 0.09 μm and an average $N_i/A_{flat}$ of 43 snowballs per 100 μm$^2$ with a standard deviation of 4 snowballs per 100 μm$^2$ (excluding 1 outlier of 64 snowballs per 100 μm$^2$).

### 3.2.2 Digital 3D Microscope Analysis Method

The 3D microscope used to capture images of the treated copper foil was a Hirox KH-8700 E (Figure 3.8).

Figure 3.8 Hirox KH-8700 E 3D Digital Microscope.

A magnification of 2800x was chosen since it provided the clearest image. One factor that proved difficult to overcome was vibration. The base of the microscope features a vibration absorber and the included software offers a digital signal processing (DSP) anti-vibration filter that provided some needed stability, but the setup could benefit from additional support from something like an isolated anti-vibration table. Again, 5 samples from 5 positions across the entire width of two rolls of copper foil, 1 treated drum side and 1 treated matte side were analyzed.

After the microscope images were captured, the system's accompanying software was used to identify the snowballs and determine the distribution of their radii. With measurement and image processing tools built in to provide a complete solution, this is certainly a convenient option. In particular, the software provides a particle counter. Unfortunately, the only algorithms provided for counting particles (or in this case snowballs) is binarization or RGB thresholding. Nonetheless, after images were captured, the provided software was used to identify the snowballs using binarization (Figure 3.9).

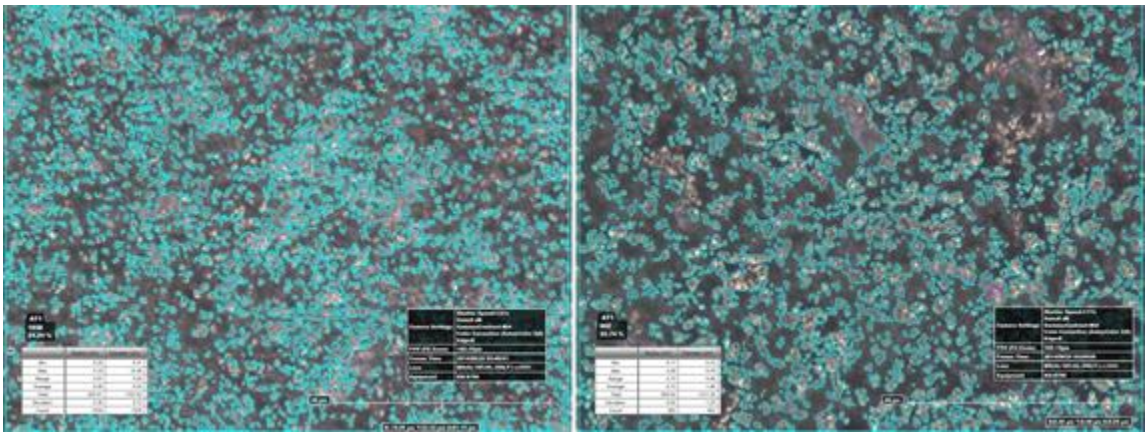

Figure 3.9 Microscope Snowballs on Drum (left) and Matte (right) Sides.

Unlike the MATLAB process, it was necessary to manually tune the binarization filters to qualitatively isolate the snowballs for each image. This can be time consuming and disrupts the automation process. As well, using different settings for each measurement decreases measurement precision (or repeatability), which could lead to increased standard deviation between similar measurements. Furthermore, Figure 3.9 provides a good example of how some snowballs are missed in the "background" while snowballs in the "foreground" are often clumped together when using binarization to count snowballs. Although the system's software cannot directly determine the snowball distribution, it does provide some immediate calculated statistics such as the total area ratio which can be used to improve the precision between measurements. Furthermore, the software allows all of the data and any measurements to be exported as a csv file. What's particularly nice about this capability is that it provides visibility of each measurement. Therefore, impractically large or small measured radii can be filtered out. However, there are 2 caveats to filtering this data. First, though this process may eliminate outlier radii, it will also eliminate the total number and thus total surface area of

the snowballs. Second, there is no inherent justification for choosing which radii are actually too large or too small. In consideration for the stated limitations and caveats, two results are provided. Both results used the previous SEM measurements to justify filtering all radii less than 0.3 μm and greater than 2 μm. Snowball counting and distribution binning was then performed with MATLAB (Figure 3.10).

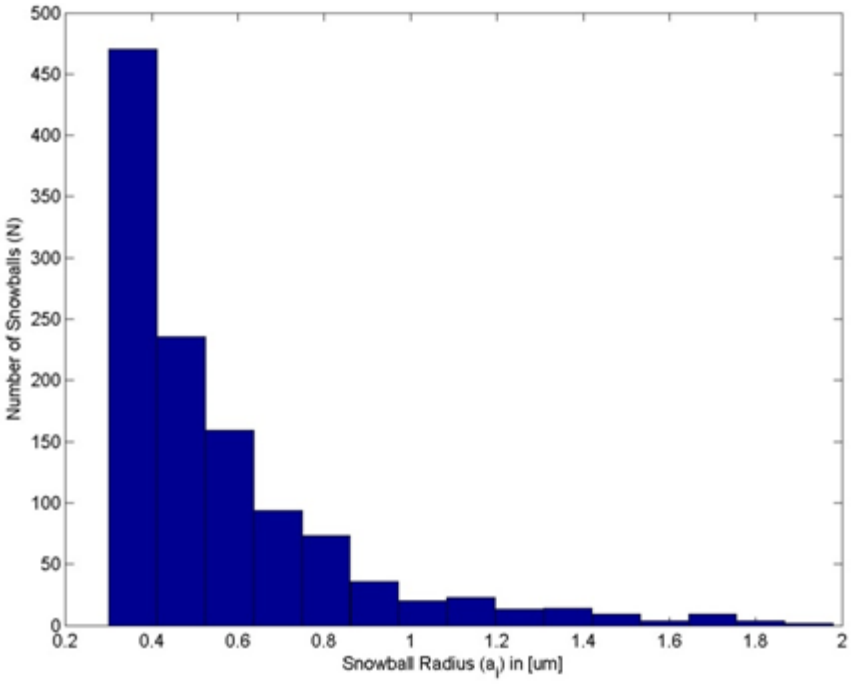


Figure 3.10 Snowball Radii Distribution of Drum Side from Microscope Method.

With no further adjustments or filtering other than what was previously stated, the drum side analysis determined an average $a_i$ of 0.59 μm with a standard deviation of only 0.03 μm and an average $N_i/A_{flat}$ of 11 snowballs per 100 μm$^2$ with a standard deviation of 4 snowballs per 100 μm$^2$. Matte side analysis determined an average $a_i$ of 0.70 μm with a standard deviation of 0.08 μm and an average $N_i/A_{flat}$ of 10 snowballs per 100 μm$^2$ with a standard deviation of 3 snowballs per 100 μm$^2$.

Since most, if not all, of the large radii previously filtered out to determine the snowball radii distribution were potentially neighbor snowballs clumped together during binarization, the distribution of snowballs was scaled to match the total area measured (i.e. the unfiltered area) in an attempt to recover surface area lost during filtering without skewing the distribution. This process does not change the value of $a_i$ or its standard deviation but $N_i/A_{flat}$ does change. The scaled drum side analysis determined 12 snowballs per 100 μm$^2$ with a standard deviation of 4 snowballs per 100 μm$^2$. The scaled matte side analysis determined 11 snowballs per 100 μm$^2$ with a standard deviation of 2 snowballs per 100 μm$^2$. Clearly this approach did not make a significant difference.

Although the microscope data for $a_i$ closely correlated with the SEM method, it is difficult to know how accurate the method would be with other foils since the binarization method seemed to miss a significant number of snowballs, as evident from a comparison of $N_i/A_{flat}$ between the microscope and SEM methods as well as Figure 3.9. Furthermore, the correlation for $a_i$ was not too surprising since any radius measurement less than 0.3 μm or greater than 2 μm was intentionally filtered out, which was ultimately justified using SEM measurements. None the less, with a few small improvements such as an anti-vibration table, a CHT method for particle counting and the inclusion of statistical software capable of providing a distribution within the system, this method can provide a convenient approach.

### 3.3 Characterizing Untreated Copper Foil: $A_{matte}/A_{flat}$

There are 2 methods presented to obtain the $A_{matte}/A_{flat}$ parameter of an untreated copper surface. The first method uses a mechanical profilometer (or perthometer) to measure the length, including all of the surface irregularities, in the x and

y dimensions to calculate the area. The second method uses a stack of images to create a quasi-three-dimensional image taken by a 3D digital microscope and measured using built-in software.

All measurement methods require some method of interpolating the distance between the measured discrete data points. There are 4 interpolation methods presented, which includes a minimum length, an effective maximum length and 2 intermediate lengths. The first interpolation is a simple linear interpolation using the Pythagorean Theorem to define the absolute minimum possible length between 2 points

$$Length_{min} = \sqrt{(Flat\ Length)^2 + (Height)^2} \tag{14}$$

shown in Figure 3.11.

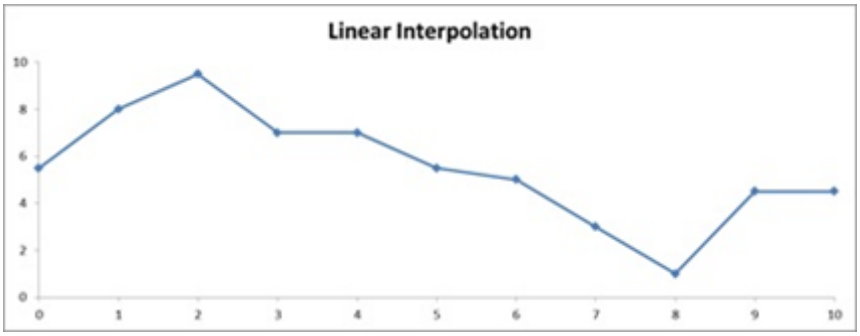


Figure 3.11 Linear Interpolation between Data Points (Absolute Minimum).

The second interpolation method calculates the arc length of a sine wave from 0 to $\pi/2$. This was considered a maximum length since it assumes a non-linear path between all points. In truth, this is not an absolute maximum. If the distance between the points is small, in this case less than 1 μm, this would provide a reasonable maximum estimate. However, as the data points move farther apart, this consideration breaks down since there is a higher probability for larger deviations and hence longer path lengths.

Since all of the step sizes between measurements were significantly less than 1 μm, it was considered the maximum length between points. The formula for calculating a non-linear arc length is

$$arc\ length = \int \sqrt{1 + \left(\frac{dy}{dx}\right)^2}\, dx \tag{15}$$

A simple method of implementing (15) for a sin interpolation is to use Simpson's Rule

$$\text{arc length} = \frac{\Delta x}{3}\left[f(x_0) + 2\sum_{j=1}^{n/2-1} f(x_{2j}) + 4\sum_{j=1}^{n/2} f(x_{2j-1}) + f(x_n)\right] \tag{16}$$

where $f(x_n) = \sqrt{1 + \cos^2(x_n)}$ and $n = 10$, shown in Figure 3.12.

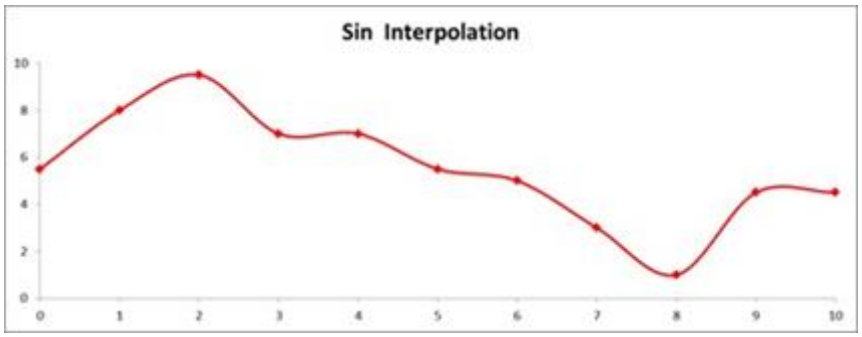


Figure 3.12 Sin Interpolation between Data Points (Effective Maximum).

The minimum and maximum interpolation methods can be used as a tool to determine whether other methods are unrealistic. The third, and **recommended**, interpolation is a hybrid of the first 2 methods. The idea behind this method is, if a linear interpolation underestimates the total length and a sin interpolation overestimates the entire length, then it's reasonable to believe the actual length is comprised of some relatively linear paths and some non-linear paths. Therefore, the hybrid interpolation uses a linear interpolation when $dz/dx = 0$ and a sin interpolation otherwise (Figure 3.13).

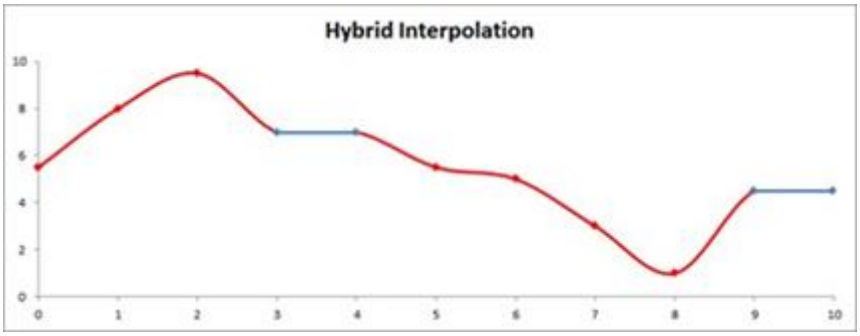


Figure 3.13 Hybrid Interpolation between Data Points (Intermediate).

The fourth method attempts to create a periodic interpolation by averaging the frequent small deviations across less frequent large deviations. This effectively acts like a low pass filter in an attempt to average the total length. There are 2 steps to implement this method. The first step is to binarize the peaks and valleys as determined by the average surface height deviation ($R_a$). The second step is to calculate the arc length of $x^2$ using (16), where $f(x_n) = \sqrt{1 + 4a^2x^2}$, $a = \left[4R_a/l_{flat}^2\right]$ and $n = 10$ (Figure 3.14).

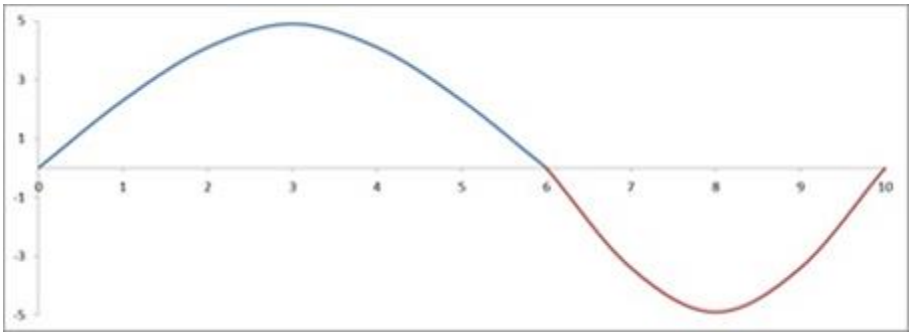

Figure 3.14 Periodic Interpolation of Data Points (Intermediate).

### 3.3.1 Mechanical Profilometer (Perthometer) Method

The perthometer used to measure the surface profile was a Mahr M2 (Figure 3.15).

Figure 3.15 Mahr M2 Perthometer Controller (left) and Pull Force Meter (right).

As mentioned, width and length measurements are needed to calculate the area. The perthometer does not record discrete data points or automatically calculate the total length. However, it will print a scaled profile on a receipt (Figure 3.16).

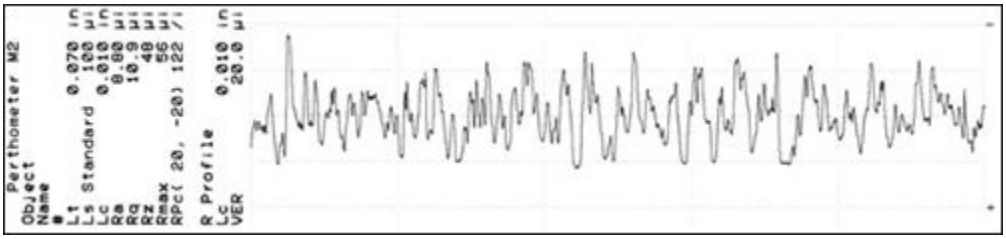


Figure 3.16 Printed Perthometer Surface Profile of Raw Untreated Copper Foil.

After the length and width measurements are obtained, the receipts need to be digitally scanned and converted to discrete data points (Figure 3.17). In order to get a step size between points of 0.335 µm, the receipts were scanned with a resolution of 600ppi.

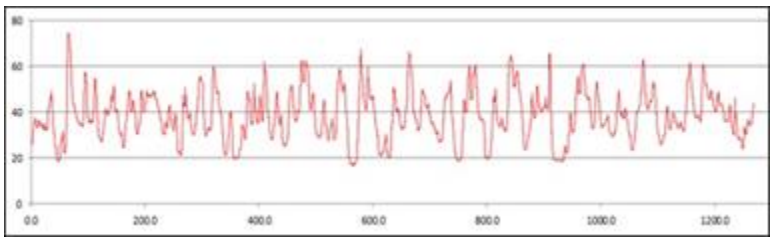


Figure 3.17 Recreation of Surface Profile from Discrete Data Points.

All 4 interpolation methods were implemented in Python and calculated on the fly during data discretization. Ten samples from both sides of raw untreated copper, drum and matte sides, were analyzed from 5 positions across the entire width of two rolls of copper foil. Results for $A_{matte}/A_{flat}$ using the perthometer method were as follows:

Table 3.1 Drum Side $A_{matte}/A_{flat}$

| Interpolation | Linear | Sin | Hybrid | Periodic |
|---|---|---|---|---|
| **Average** | 1.0224 | 1.0758 | 1.0549 | 1.0222 |
| $\boldsymbol{\sigma_s}$ | 0.003 | 0.003 | 0.003 | 0.006 |

Table 3.2 Matte Side $A_{matte}/A_{flat}$

| Interpolation | Linear | Sin | Hybrid | Periodic |
|---|---|---|---|---|
| **Average** | 1.1095 | 1.1674 | 1.1455 | 1.1165 |
| $\boldsymbol{\sigma_s}$ | 0.006 | 0.007 | 0.007 | 0.028 |

The periodic interpolation method was found to unrealistically underestimate lengths and consequently the area, and had the largest standard deviation. Therefore, the **recommended method is the hybrid method**. One possible concern for the perthometer method is that it assumes the same length and width profiles exist across the entire area. However, if this assumption were incorrect it would likely result in a large standard deviation, where these measurements showed only small standard deviations. One way to test this assumption and/or improve the accuracy would be to use an optical profilometer. The methods outlined for a mechanical profilometer can be used directly to calculate the

area between all the data points and summing the complete area like a grid. This would reduce uncertainty of the measurement to a much smaller area, increasing the overall accuracy.

### 3.3.2 Digital 3D Microscope Analysis Method

The same 3D microscope used to determine $a_i$ and $N_i/A_{flat}$, a Hirox KH-8700 E, was also used to determine $A_{matte}/A_{flat}$. This analysis requires the microscope to capture a quasi-3D image of the surface by taking several images at different focal lengths and stacking them, which is a simple automated process (Figure 3.18).

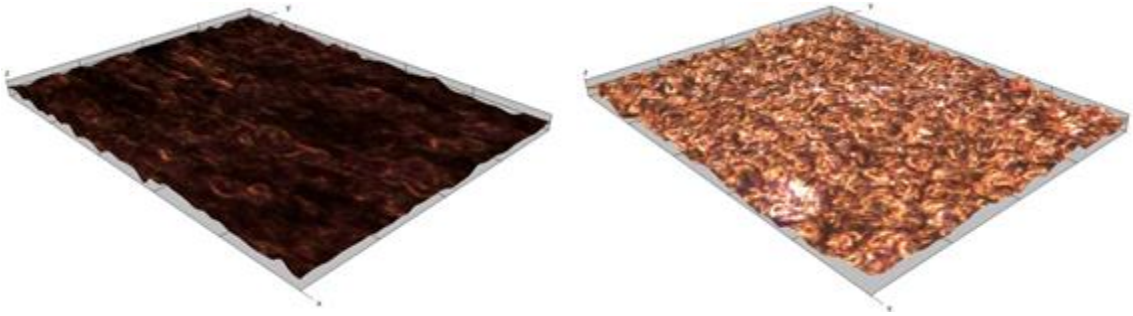

Figure 3.18 3D Drum Side (left) and Matte Side (right) Untreated Copper Surfaces.

Analysis is made easy using the built-in volume measurement software by setting the range and simply clicking on the surface. The software's interpolation algorithm between data points is undetermined. However, the measurement step size can be determined by exporting the data as a csv file, which in this case was 0.057 μm. Five samples from both sides of raw untreated copper, drum and matte sides, were analyzed from 5 positions across the entire width of two rolls of copper foil. Drum side analysis determined an average $A_{matte}/A_{flat}$ of 1.13 with a standard deviation of 0.028. Matte

side analysis determined an average $A_{matte}/A_{flat}$ of 1.17 with a standard deviation of 0.022.

Again, the vibration proved difficult to overcome for this measurement. The number of focal lengths was set to 15 intervals but it can be set higher to reduce the step size in the z-axis and improve the resolution. Beyond 15 intervals, the anti-vibration DSP filter was unable to properly compensate and caused the image to distort. As well, the vibration likely shifted the X-Y plane between focal lengths, further degrading accuracy of the measurements. This may explain the larger surface areas and increased standard deviation as compared to the perthometer method. It also seems unlikely that there is only a 4% difference in surface area between the drum and matte sides. Still, this is a very simple and convenient method that could likely improve its results with an anti-vibration table.

# CHAPTER 4

## USING CHARACTERIZED PARAMETERS IN SIMULATION TOOLS

Much of the text and images in this chapter have been submitted for a technical conference paper and presentation [22]. As concluded previously, all snowball radii should be determined entirely and described as a distribution, since power loss can change as a function of distribution and standard deviation. Although that conclusion is correct, only a single radius can be used in existing commercially available simulation tools to guarantee a causal impedance boundary function [15]

$$\frac{P_{rough}}{P_{smooth}} \approx 1 + \left(\frac{3}{2}\right)(SR)\left(\frac{1}{1+\frac{\delta(f)}{a}+\frac{1}{2}\left(\frac{\delta(f)}{a}\right)^2}\right) \tag{17}$$

where $SR$ is the Hall-Huray Surface Ratio [16]

$$SR = \frac{4\pi N a^2}{A_{flat}} \tag{18}$$

One concern as previously described for using a single radius rather than a radii distribution is minor deviations as a function of frequency. Such deviations are often negligible for practical purposes under 100 GHz, but can be improved with a distribution. Also, the assumption made by (17) that $A_{matte}/A_{flat} = 1$ may underestimate conductor losses under a few GHz, depending on how close the untreated surface is to being perfectly flat. The approach is then to determine a single "effective" radius that best represents the impact of the complete snowball distribution and untreated surface area on total power loss.

## 4.1 An Effective Snowball Radius

Implementation of (17) requires that a single **effective** snowball radius be determined, which is not the same as determining the **average** snowball size. To clarify, depending on how the calculation is performed, there may be 2 different averages. An absolute average is determined by averaging all of the measured snowball radii. A bin average is determined by averaging the range or distribution bins. All previously reported averages were the absolute averages. There are then 3 different radii: an '**absolute average radius**', a '**bin average radius**', and an '**effective radius**'.

In order to compare the characterization methods and snowball model predictions to actual insertion loss measurements, the SEM analysis method was used to characterize the snowball distribution of a single image of ED foil manufactured by Gould (Figure 2.15) to correspond with VNA measurements previously obtained by [7]. Characterization obtained a distribution for $N_i/A_{flat}$ with a total density $N_{total}/A_{flat}$ of 32 snowballs per 90 μm$^2$ (Figure 4.1).

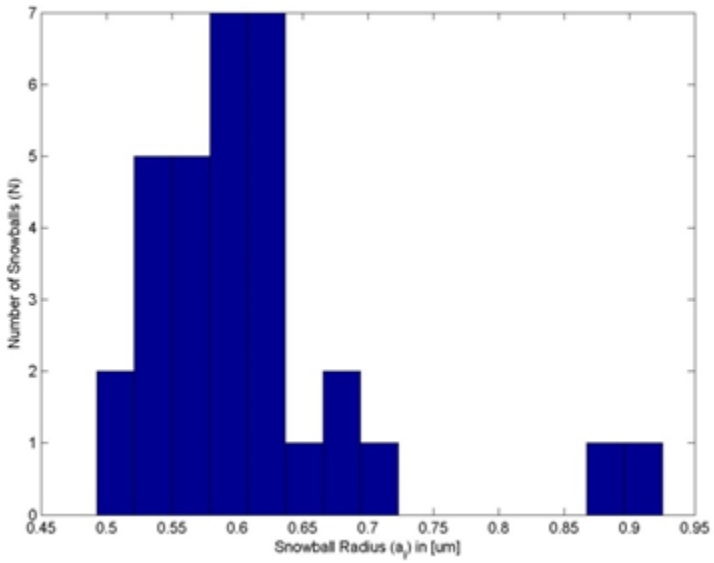


Figure 4.1 Gould Snowball Radii Distribution of Drum Side from SEM Method.

The value for $A_{matte}/A_{flat}$ was assumed to be the same as the Oak-Mitsui copper of 1.055from the recommended hybrid interpolation results in Table 3.1 since a sample of untreated Gould copper was not available. Equation (8) was then calculated for the complete distribution across 15 bins and subsequently calculated for a single **absolute average radius** of 0.6 μm as well as a **bin average radius** of 0.7 μm, all using the same total snowball density $N_{total}/A_{flat}$ of 32 snowballs per 90 μm$^2$. A single **effective radius** as it pertains to $SR$, was then calculated with the same total snowball density $N_{total}/A_{flat}$ of 32 snowballs per 90 μm$^2$, only this time $A_{matte}/A_{flat}$ was set to 1 to agree with (17), and the **effective radius** $a_{effective}$ was manually tuned until the effective curve best matched the complete distribution curve at 0.63 μm (Figure 4.2).

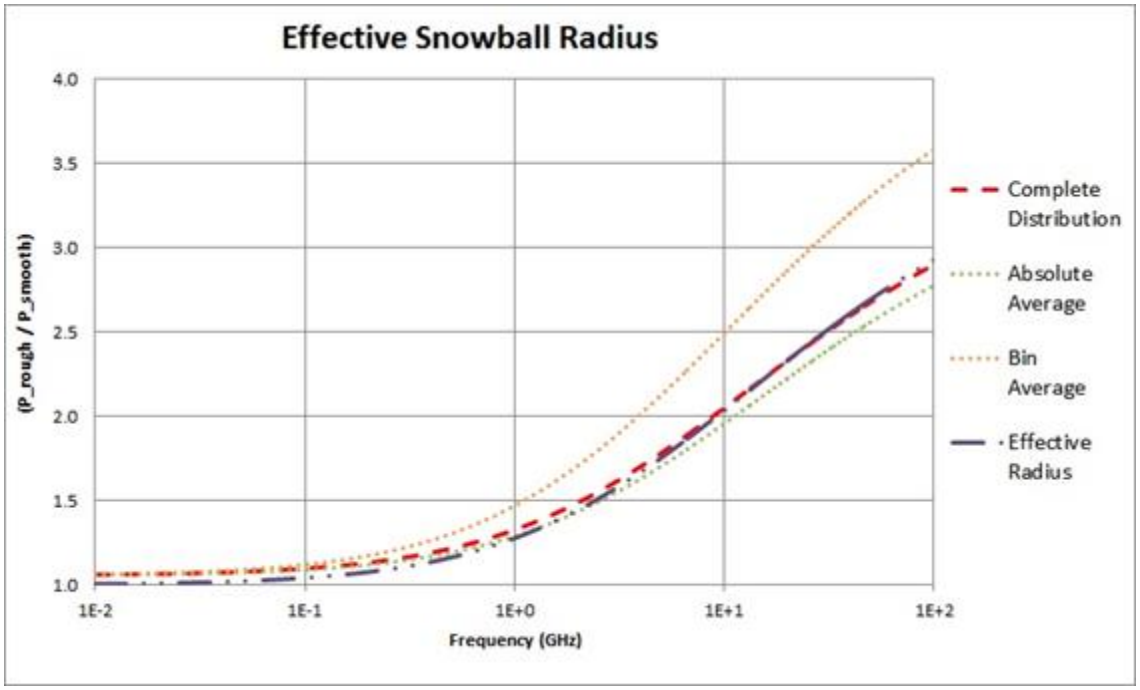


Figure 4.2 Determination of an Effective Snowball Radius.

In this instance, the **absolute average radius** tended to slightly underestimate the impact of the snowballs at high frequencies, while the **bin average radius** tended to overestimate. The proximity of the complete distribution and absolute average curves were caused by the skewed distribution of the snowballs which may change with products and vendors, and thus does not conflict with or supersede Figure 3.1. One convenient relationship between the complete distribution and **effective radius** curves worth noting is a single cross-over frequency. This metric could be leveraged to easily automate the process of fitting the effective radius curve to the complete distribution curve by selecting an appropriate cross-over frequency as an algorithm condition. The 2 parameters necessary to define the finite conductivity boundary in simulation for this particular copper foil were then: an **effective radius** of 0.63 μm and a corresponding **Hall-Huray Surface Ratio** of 1.77 from (18).

### 4.2 Performance Experiments

To evaluate the accuracy of the **effective radius** and its corresponding **Hall-Huray Surface Ratio** as determined in the previous section, 5" and 7" single-ended microstrips were modeled in Ansys® HFSS™ for insertion loss predictions and compared to actual VNA insertion loss measurements from the same test boards used by [7]. Microstrip and substrate dimensions of [7] were determined as previously measured by [17] (layer 6 - bottom layer) (Table 4.1). The dielectric constant and dissipation factor were $\varepsilon_r = 3.78$ and $\tan\delta = 0.086$ at 2 GHz, as determined from the manufacturer's specifications [18]. The dimensions were modeled exactly and a solder mask was added as illustrated in [17], with $\varepsilon_r = 3.5$ and $\tan\delta = 0.025$ at 7 GHz [15] (Figure 4.3).

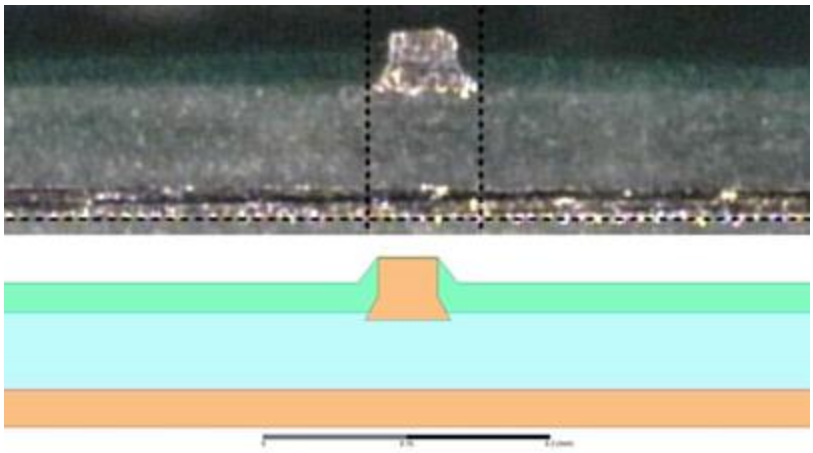

Figure 4.3 Actual Microstrip (top) and Modeled Microstrip (bottom).

Table 4.1 Microstrip Model Dimensions

| Feature | Size |
|---|---|
| **Trace Width (top)** | 2.4579 mils |
| **Trace Width (bottom)** | 3.6256 mils |
| **Trace Thickness** | 2.5746 mils |
| **Substrate Thickness** | 2.8957 mils |
| **Ground Thickness** | 1.3907 mils |

Finally, a conductivity boundary was set for the conductor using the software's Huray Surface Roughness Model with the previously determined **effective radius** of 0.63 μm and **Hall-Huray Surface Ratio** of 1.77 before simulation. The only difference between the 5" and 7" models is the length. For comparison, HFSS offers a modified version of the Morgan-Hammerstad empirical fit, known as the Groisse equation

$$\frac{P_{rough}}{P_{smooth}} = 1 + \exp\left(-\left[\frac{\delta}{\Delta}\right]^{1.6}\right) \tag{19}$$

which also saturates at a maximum of 2.0 like the Morgan-Hammerstad empirical fit, but the Hammerstad equation saturates at a lower frequency [19]. An RMS value of 1.2 μm was used for the Groisse equation, as previously characterized in [7]. It was first simulated at 5" using a flat non-causal substrate model (Figures 4.4 and 4.5).

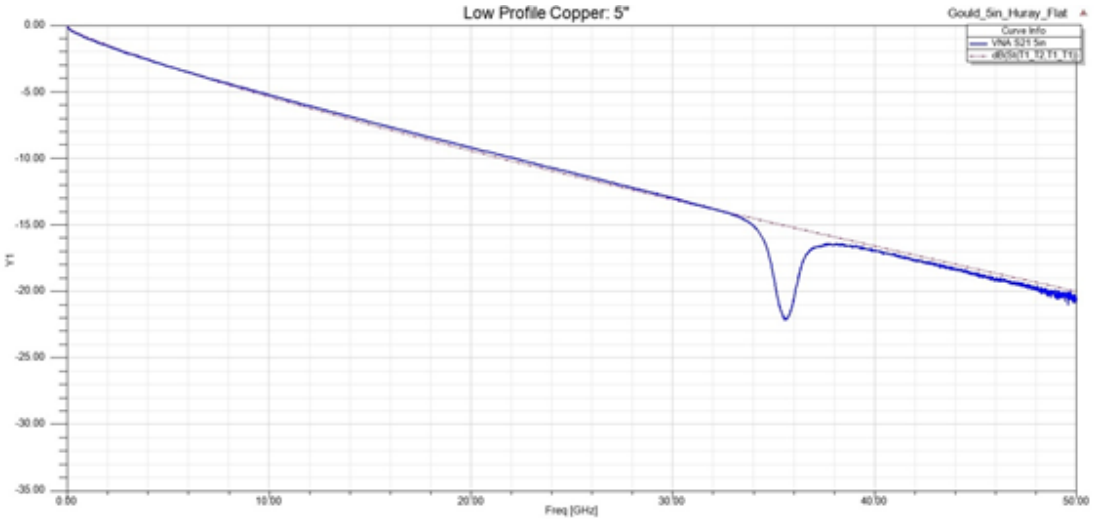


Figure 4.4 5" Huray Model with a flat non-causal substrate vs. VNA Measured.

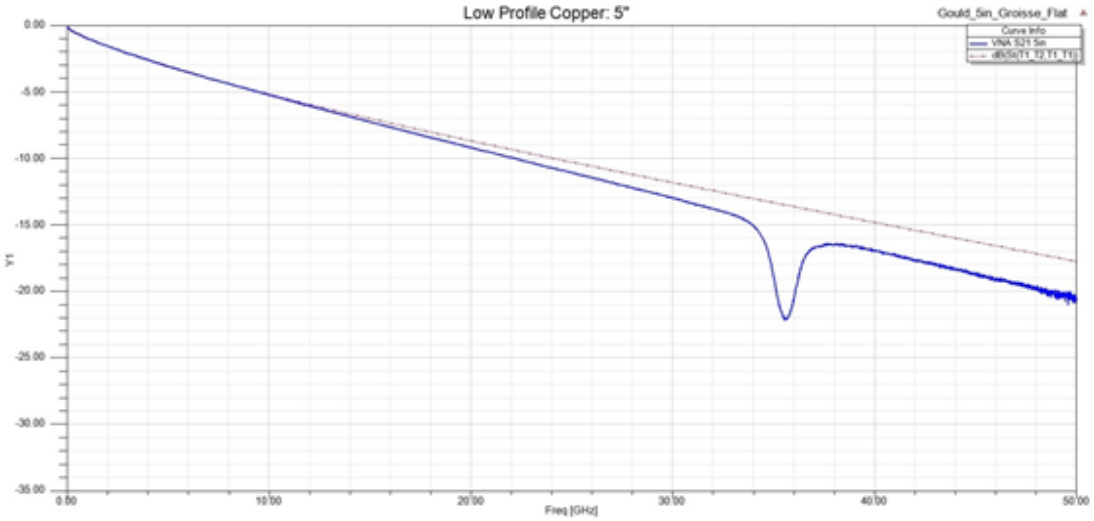


Figure 4.5 5" Groisse Model with a flat non-causal substrate vs. VNA Measured.

Figure 4.4 show a close correlation between the predicted and actual insertion losses up to 50 GHz using the Huray model with a characterized effective radius and a flat non-causal substrate model, with some expected minor deviations as a function of frequency. Figure 4.5 shows the Groisse equation was only capable of predicting up to 12 GHz for a 5" single-ended microstrip. It was then simulated at 7" using a flat non-causal substrate model (Figures 4.6 and 4.7).

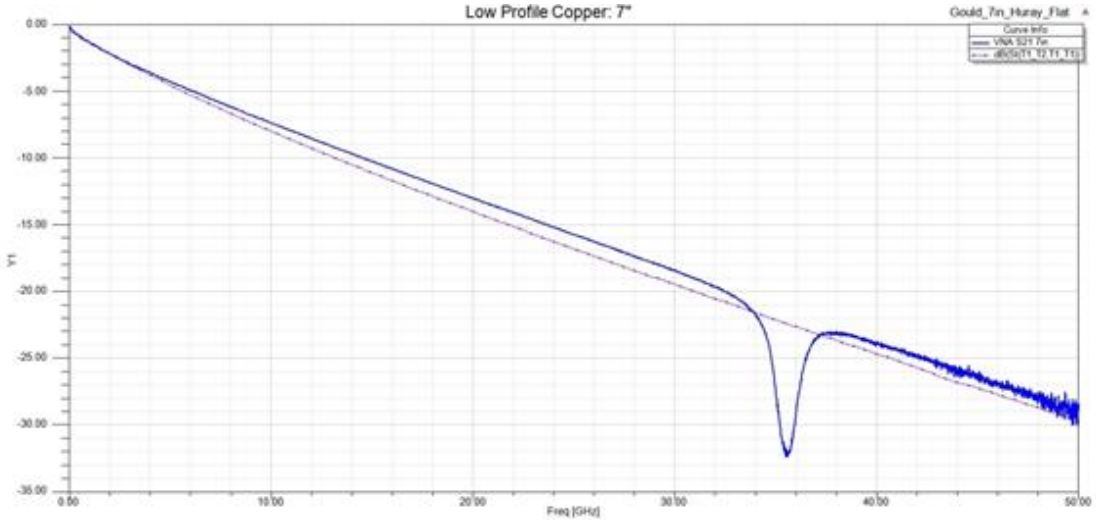


Figure 4.6 7" Huray Model with a flat non-causal substrate vs. VNA Measured.

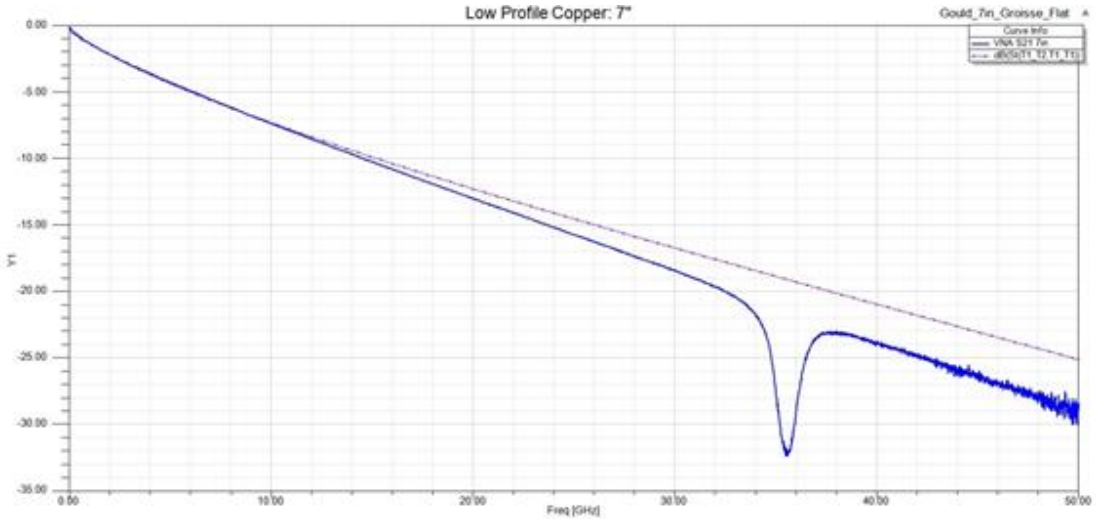


Figure 4.7 7" Groisse Model with a flat non-causal substrate vs. VNA Measured.

Figure 4.6 shows the 7” microstrip was slightly less lossy than predicted by the Huray model with a characterized effective radius and a flat non-causal substrate model, but maintained a relatively close correlation up to 50 GHz. The Groisse equation was again incapable of predicting above 12 GHz. The 5” microstrips were then simulated using a wideband Debye (Djordjevic-Sarkar) substrate model (Figures 4.8 and 4.9).

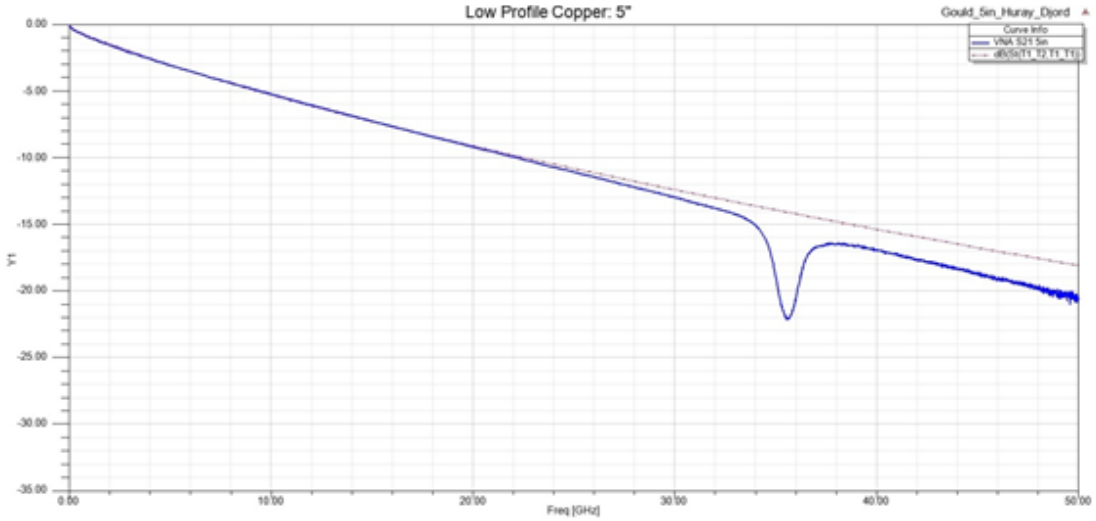


Figure 4.8 5” Huray Model with a Djordjevic-Sarkar substrate vs. VNA Measured.


Figure 4.9 5” Groisse Model with a Djordjevic-Sarkar substrate vs. VNA Measured.

Figure 4.8 shows the Huray model with a characterized effective radius was capable of predicting up to about 22 GHz for a 5” trace using a Djordjevic-Sarkar substrate model. Figure 4.9 shows the Groisse model was only capable of predicting up to about 10 GHz using the same trace and substrate. Finally, the 7” microstrips were simulated using a Djordjevic-Sarkar substrate model (Figures 4.10 and 4.11).


Figure 4.10 7” Huray Model with a Djordjevic-Sarkar substrate vs. VNA Measured.


Figure 4.11 7” Groisse Model with a Djordjevic-Sarkar substrate vs. VNA Measured.

Figure 4.10 shows the Huray model with a characterized effective radius was again capable of predicting up to about 22 GHz for a 7" trace using a Djordjevic-Sarkar substrate model. Figure 4.11 shows the Groisse model was only capable of predicting up to about 8 GHz using the same trace and substrate. It is difficult at this point to know the exact root causes for all deviations observed. Figures 4.4 – 4.11 do support the claim that the Huray model was able to improve the predicted insertion loss as compared to the Groisse equation and thus the Morgan-Hammerstad empirical fit. Although only 1 image was used to determine a snowball distribution and a subsequent effective radius, Figures 4.4 – 4.11 also suggest the characterization methods described in this thesis can yield accurate conductor loss modeling at higher frequencies as compared to conventional methods.

It is also unclear at this point if there are hidden snowballs impacting the results or whether multiple layers of snowballs would have a significant effect. Still, it was surprising how well the distribution of only a single image predicted insertion loss when compared to conventional methods. Nonetheless, it seems reasonable to believe that an analysis of several samples could obtain a more statistically reliable representation of the snowball distribution across the entire copper foil surface.

# CHAPTER 5

# DISCUSSION

## 5.1 CONCERNS AND ALTERNATIVES

A potential concern for measuring the snowball distribution from SEM images is the obtainable field of view. Since an SEM image can only reveal the surface snowballs, any snowballs hidden between the surface snowballs and the matte foil surface are undetectable. More to the point, there is no way of determining the depth of a snowball stack-up with a two-dimensional image of the surface. Therefore, a method is recommended to estimate the total volume occupied by snowballs within an area if determined necessary. This process will need to be slightly different for the drum and matte sides. For the drum side, an additional cross section image will be needed to determine the height of the stack-up. The height could in turn be used to calculate the total volume occupied by the snowballs (Figure 5.1).

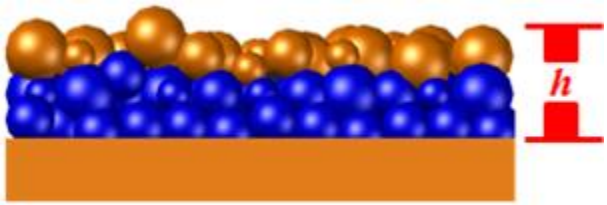


Figure 5.1 Hidden snowballs (blue) beneath surface snowballs on low profile ED foil.

Finally, the size distribution of the surface snowballs can be scaled to match the total volume occupied (Figure 5.2).

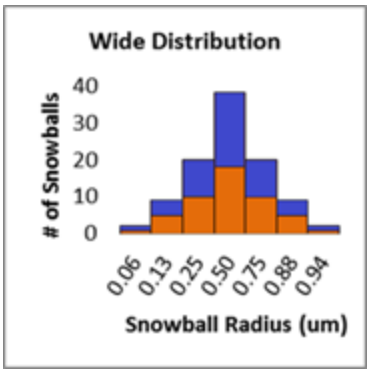


Figure 5.2 Hypothetical distribution (orange) scaled by hidden snowballs (blue).

For the matte side, it may be possible to measure the average diameter of the snowball stack-up at the peak (Figure 5.3).

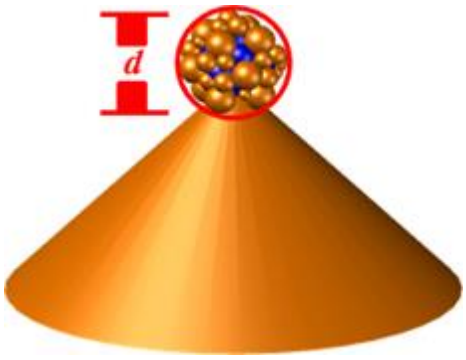


Figure 5.3 Hidden snowballs (blue) beneath surface snowballs on high profile ED foil.

This may need to be corrected if the snowball stack-up is not spherical. The diameter could in turn be used to calculate the total volume occupied by snowballs. Again, the size distribution of the surface snowballs can be scaled to match the total volume occupied (Figure 5.2).

## 5.2 Known Limitations of this Research

There are a few known limitations of these results. The first is that it ignores the elemental composition of the snowballs. While the snowballs are mostly copper, the

treatment process illustrated as the third phase in Figure 2.7, intentionally add impurities to the surface to provide a number of non-electrical properties such as anti-oxidation, anti-staining or PCB adhesion. One example is called a “treatment of brass” (TOB) which results in a surface composition of copper, carbon, oxygen, silicon, zinc, and nitrogen (Figure 5.4).

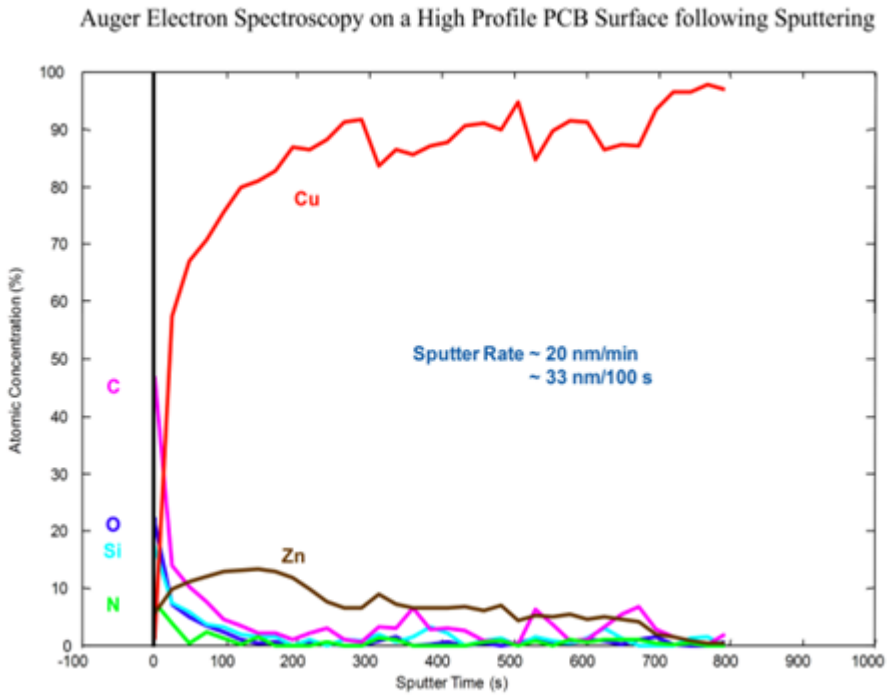


Figure 5.4 Elemental compositions of snowballs after a treatment of brass. [9]

Figure 5.4 shows how the elemental composition of a snowball changes from CuZn (brass) at the snowball surface to almost pure copper around 260 nm deep. Since the conductivity changes with each element, this can affect the snowball model’s results, especially at higher frequencies where skin depth decreases. However, many of the impurities added to ED foil are trade secrets and can therefore change from one product to another. As future skin depths become isolated within this region, each manufacturer

will need to be responsible for their own analysis in order to maintain their trade secrets. Therefore, the elemental composition of the snowballs has been deemed beyond the scope of this research.

A second limitation of this research is the assumption that dielectric loss can be accurately determined for VNA correlation. This is especially true since the dielectric used for correlation was FR-4. It has been previously established that the periodic structure of the glass weave within the resin structure can cause additional resonant losses which are not accounted for in simulation [20]. Also, common substrate materials exhibit resonant effects on signal propagation [17]. Since this research is focused on the conductor losses, this known limitation has also been deemed beyond the scope of this research.

A third limitation is that the characterization methods described cannot be performed after lamination. Although this may not have any meaningful effect on the predicted losses, it does pose a challenge to PCB manufacturers. It is unusual for manufacturers to have access to either the material or instruments needed to perform the characterization outlined by this research. None the less, this research provides a considerable milestone towards the advancement of foil characterization as it pertains to accurate conductor loss modeling in high-speed devices. It may be adopted as presented by the manufacturers themselves as the demand for this characterization increases along with higher data rate designs in the near future. It may also be used in future research to develop a solution that is available to PCB manufacturers after the lamination process; such as a hybrid between this research and other RMS surface roughness detection methods from PCB cross sectional images [21].

# CHAPTER 6

# CONCLUSION AND FUTURE WORK

## 6.1 CONCLUSION

This thesis demonstrated a few methods of directly characterizing electrodeposited copper foil surface roughness to obtain snowball model parameters for accurate conductor loss modeling. The characterized parameters include $A_{Matte}/A_{Flat}$, $a_i$, and $N_i/A_{Flat}$. In doing so, this research has advanced the existing body of literature on high-speed conductor losses by improving the description of geometric surface profiles for electrodeposited copper foil as well as providing industry with the first steps to directly implement the snowball model. Additionally, this thesis further legitimized the analytic form of the snowball model as it pertains to scattered power, demonstrated the practical impact of its parameters, and revealed a source of existing irregularities between the estimated model parameters and actual performance measurements.

Furthermore, a method of determining a single effective snowball radius, $a_{effective}$ using $N_{total}/A_{Flat}$, was presented to implement the snowball model in existing commercially available field simulator software. Particular attention was paid to the value of ascertaining a complete distribution of snowball radii and how to determine the most effective radius to best represent the impact of the entire snowball distribution and untreated surface area on conductor loss. Simulation experiments, while limited, still demonstrated reasonable power loss predictions up to 50 GHz using a characterized snowball distribution and effective snowball radius with the snowball model.

## 6.2 Future Work

The next step could be to fabricate new test boards using the same electrodeposited foil characterized in this thesis to measure insertion loss for comparison with these results. A low loss substrate without periodic structures, such as polytetrafluoroethylene (PTFE) would be preferred to better isolate the conductor loss from the substrate loss. A foil cross section analysis could provide a method of characterizing multiple snowball layers to determine whether they exist and if they have any significant impact on conductor loss. If cross section images can be obtained with reasonable snowball visibility, the methods outlined in this thesis could be extended to analyze a PCB cross section for a post lamination characterization. While perhaps time consuming and simulation intensive, it would be interesting to model the snowballs explicitly in a field simulator and explore the results. Finally, the impact of the elemental composition of the snowballs is still undetermined.

## REFERENCES


[1] Intel, "Intel Chips," [Online]. Available: http://www.intel.com/content/dam/www/public/us/en/documents/corporate-information/history-intel- chips-timeline-poster.pdf

[2] B. Lee *et al.*, "Design Optimization for Minimal Crosstalk in Differential Interconnect," *DesignCon 2012*, vol. 2, 2012, pp. 1263-1292

[3] S. Morgan, "Effect of Surface Roughness on Eddy Current Losses at Microwave Frequencies," *Journal of Applied Physics*, vol. 20, 1949, pp. 352-362

[4] E. Hammerstad and F. Bekkadal, "Microstrip Handbook," *ELAB-report, STF44 A74169*, Trondheim, Feb. 1975

[5] E. Hammerstad and O. Jensen, "Accurate Models for Microstrip Computer-Aided Design," *Microwave symposium Digest, IEEE MTT-S International*, May 1980, pp.407-409

[6] S. Hall *et al*., "Modeling Requirements for Transmission Lines in Multi-Gigabit Systems," *Electrical Performance of Electronic Packaging, 2004. IEEE 13th Topical Meeting*, Oct 2004, pp. 67-70

[7] O. Oluwafemi, "Surface Roughness and its Impact on System Power Losses," Ph.D. dissertation, Dept. of Elec. Eng., Univ. of South Carolina, Columbia, SC 2007

[8] P. Huray *et al.*, "Impact of Copper Surface Texture on Loss: A Model that Works," *DesignCon 2010*, vol. 1, 2010, pp. 462-483

[9] P. Huray, *The Foundations of Signal Integrity*. Hoboken, NJ: John Wiley & Sons, Inc., 2010, pp. 109-144, 216-276

[10] E. Bogatin *et al.*, "Which one is better? Comparing Options to Describe Frequency Dependent Losses," DesignCon 2013, vol. 1, 2013, pp. 469-494

[11] H. Kuba *et al.*, "Automatic Particle Detection and Counting By One-Class SVM From Microscope Image," *Proc. Int. Conf. on Neural Information Processing, Lecture Notes in Computer Science*, vol.5507, 2009, pp. 361-368

[12] M.Block and R.Rojas, "Local Contrast Segmentation to Binarize Images," in *Proc. of the 3rd International Conference on Digital Society (ICDS 2009)*, vol.1, no.1, Cancun, Mexico, 2009, pp.294-299

[13] C. Labno, "Two Ways to Count Cells with ImageJ," [Online]. Available: http://digital.bsd.uchicago.edu/resources_files/cell%20counting%20automated%20and%20manual.pdf

[14] T. Atherton and D. Kerbyson, "Size invariant circle detection," Image and Vision Computing, Vol. 17, no. 11, 1999, pp. 795-803

[15] J. Bracken, "A Causal Huray Model for Surface Roughness," DesignCon 2012, vol. 4, 2012, pp. 2880-2914

[16] Ansys, Inc., "HFSS™ Online Help," pp. 19.104-19.109. [Online]. Available: https://support.ansys.com/portal/site/AnsysCustomerPortal/template.fss?file=/prod_docu/15.0/ebu/hfss_onlinehelp.pdf
[17] C. Jones, "Measurement and analysis of high frequency resonances in printed circuit boards," MS dissertation, Dept. of Elec. Eng., Univ. of South Carolina, Columbia, SC 2010
[18] Isola, "IS620 Typical Laminate Properties." [Online]. Available: http://advantage-dev.com/services/docs/Isola%20IS620rev2.pdf
[19] A. Horn *et al.*, "Effect of conductor profile on the insertion loss, phase constant, and dispersion in thin high frequency transmission lines," DesignCon 2010, vol. 1, 2010, pp. 440-461
[20] P. Pathmanathan, "Power Loss due to Periodic Structures in High-Speed Packages and Printed Circuit Boards," *Microelectronics and Packaging Conference (EMPC), 2011 18th European*, 12-15 Sept. 2011, pp.1-8
[21] S. De *et al.*, "Semi-Automatic Copper Foil Surface Roughness Detection from PCB Microsection Images," *2012 IEEE International Symposium on Electromagnetic Compatibility (EMC)*, 6-10 Aug. 2012, pp.132-137
[22] M. Griesi *et al.*, "Electrodeposited Copper Foil Surface Characterization for Accurate Conductor Loss Modeling," *DesignCon 2015*, 2015

## **APPENDIX A** – PERIODIC INTERPOLATION PSEUDOCODE

1. Find $R_z$ from all data points.
2. Use Boolean operator to identify number of peaks and valleys (defined $R_z/2$) for a cross section in 1 plane.
3. Measure the length of each peak or valley (resolution*N data points) and average for $l_{flat}$.
4. Repeat for each cross section to find average number of peaks and valleys along with their average lengths.
5. Create a periodic representation of average peaks and valleys per unit length for $l_{matte}/l_{flat}$.
6. Calculate 1 positive and negative arc length using their respective average lengths and a maximum $R_z$ peak.
7. Multiply by the respective number of peaks and valleys for desired $l_{flat}$.
8. Repeat steps 1-6 for other plane.
9. The product of steps $7 * 8 = \frac{A_{matte}}{A_{flat}}$.

## **APPENDIX B** – MATLAB CODE FOR OAK-MITSUI IMAGE ANALYSIS

```
% Count & Measure Snowballs
clear;
warning('off','images:initSize:adjustingMag'); % Suppress image size warning
warning('off','images:imfindcircles:warnForLargeRadiusRange'); % Suppress circle
radius range warning
warning('off','images:imfindcircles:warnForSmallRadius'); % Suppress circle radius
minimum warning
folder = 'Images/'; % Image Folder
titleName = input('Enter JPG image file name: ', 's');
fileName = strcat(folder,titleName,'.jpg');
semIn = imread(fileName); % Read Image
semIn = imresize(semIn,850/size(semIn,2)); % Maximize Image
figure; % Open New Figure Window
imshow(semIn,'Border','tight'); % Show Scaled Image
measureDist = imdistline; % Show Line Tool
scalePix = input('Measure the length of the scale with the line tool and enter: ');
scaleLin = input('Enter the actual scale value: ')/scalePix; % Calculate Pixel-to-Linear
Conversion Factor
scaleUnit = input('Enter the scale units: ', 's');
delete(measureDist); % Remove Line Tool
```

```
measureDist = imdistline; % Show Line Tool
cropIm = input('Measure from the top of the image to the top of the bottom info border
with the line tool and enter: ');
semIn = imcrop(semIn,[0 0 size(semIn,2) cropIm]); % Crop Image
delete(measureDist); % Remove Line Tool
close(figure,1); % Close Figure Window
snowballImage = figure; % Open New Figure Window
imshow(semIn,'Border','tight'); % Show Cropped Image
measureDist = imdistline; % Show Line Tool
radiusSmall = floor(input('Measure the diameter of the smallest snowball with the line
tool and enter: ')/2);
delete(measureDist); % Remove Line Tool
measureDist = imdistline; % Show Line Tool
radiusLarge = ceil(input('Measure the diameter of the largest snowball with the line tool
and enter: ')/2);
delete(measureDist); % Remove Line Tool
[centerLocation, radiiPix] = imfindcircles(semIn,[radiusSmall
radiusLarge],'ObjectPolarity','bright','Sensitivity',0.95,'Method','twostage','EdgeThreshold
',0.25); % Find Circles
results = viscircles(centerLocation,radiiPix); % Draw Circles
radiiLin = radiiPix*scaleLin; % Convert pixel radii to linear radii
histogramImage = figure; % Open New Figure Window
hist(radiiLin, 15); % Display histogram of snowball sizes in 15 bins
```

```
histTitle = strrep(titleName,'_','.'); % Format Histogram Title
title(textwrap(strcat('Snowball Distribution for',{' '},histTitle),30)); % Histogram Title
xlabel(strcat('Snowball Radius (a_i) in [',scaleUnit,'])); % Histogram X-axis Label
ylabel('Number of Snowballs (N)'); % Histogram Y-axis Label
[N, ai] = hist(radiiLin, 15); % Store snowball distribution
totalSnowballs = sum(N); % Total number of snowballs
avgSnowballRadius = mean(radiiLin); % Average size of snowballs
saveas(snowballImage,char(strcat('Results/',titleName,{' '},'- Snowballs')),'png'); % Save
Snowball Image
close(snowballImage);
saveas(histogramImage,char(strcat('Results/',titleName,{' '},'- Histogram')),'png'); % Save
Histogram Image
close(histogramImage);
xlName = char(strcat('Results/',titleName,{' '},'- Data','.xlsx')); % Excel File Name
%Store Data in Excel Spreadsheet
xlswrite(xlName,strcat({'Average Snowball Radius in ['},scaleUnit,{']'}),'Sheet1','A1');
xlswrite(xlName,avgSnowballRadius,'Sheet1','A2');
xlswrite(xlName,{'Total Number of Snowballs'},'Sheet1','B1');
xlswrite(xlName,totalSnowballs,'Sheet1','B2');
xlswrite(xlName,strcat({'Snowball Size (a_i) in ['},scaleUnit,{']'}),'Sheet1','A4');
xlswrite(xlName,transpose(ai),'Sheet1','A5:A19');
xlswrite(xlName,{'Number of Snowballs (N_i)'},'Sheet1','B4');
xlswrite(xlName,transpose(N),'Sheet1','B5:B19');
```

## APPENDIX C – MATLAB CODE FOR GOULD IMAGE ANALYSIS

```
% Count & Measure Snowballs

clear;

warning('off','images:initSize:adjustingMag'); % Suppress image size warning

warning('off','images:imfindcircles:warnForLargeRadiusRange'); % Suppress circle
radius range warning

warning('off','images:imfindcircles:warnForSmallRadius'); % Suppress circle radius
minimum warning

folder = 'Images/'; % Image Folder

titleName = input('Enter JPG image file name: ', 's');

fileName = strcat(folder,titleName,'.jpg');

semIn = imread(fileName); % Read Image

semIn = imresize(semIn,850/size(semIn,2)); % Maximize Image

snowballImage = figure; % Open New Figure Window

imshow(semIn,'Border','tight'); % Show Scaled Image

measureDist = imdistline; % Show Line Tool

scalePix = input('Measure the length of the scale with the line tool and enter: ');

scaleLin = input('Enter the actual scale value: ')/scalePix; % Calculate Pixel-to-Linear
Conversion Factor

scaleUnit = input('Enter the scale units: ', 's');
```

```
delete(measureDist); % Remove Line Tool
measureDist = imdistline; % Show Line Tool
radiusSmall = floor(input('Measure the diameter of the smallest snowball with the line
tool and enter: ')/2);
delete(measureDist); % Remove Line Tool
measureDist = imdistline; % Show Line Tool
radiusLarge = ceil(input('Measure the diameter of the largest snowball with the line tool
and enter: ')/2);
delete(measureDist); % Remove Line Tool
[centerLocation, radiiPix] = imfindcircles(semIn,[radiusSmall
radiusLarge],'ObjectPolarity','bright','Sensitivity',0.94,'Method','twostage','EdgeThreshold
',0.1); % Find Circles
results = viscircles(centerLocation,radiiPix); % Draw Circles
radiiLin = radiiPix*scaleLin; % Convert pixel radii to linear radii
histogramImage = figure; % Open New Figure Window
hist(radiiLin, 15); % Display histogram of snowball sizes in 15 bins
histTitle = strrep(titleName,'_','.'); % Format Histogram Title
title(textwrap(strcat('Snowball Distribution for',{' '},histTitle),30)); % Histogram Title
xlabel(strcat('Snowball Radius (a_i) in [',scaleUnit,'])); % Histogram X-axis Label
ylabel('Number of Snowballs (N)'); % Histogram Y-axis Label
[N, ai] = hist(radiiLin, 15); % Store snowball distribution
totalSnowballs = sum(N); % Total number of snowballs
avgSnowballRadius = mean(radiiLin); % Average size of snowballs
```

```
saveas(snowballImage,char(strcat('Results/',titleName,{' '},'- Snowballs')),'png'); % Save
Snowball Image
close(snowballImage);
saveas(histogramImage,char(strcat('Results/',titleName,{' '},'- Histogram')),'png'); % Save
Histogram Image
close(histogramImage);
xlName = char(strcat('Results/',titleName,{' '},'- Data','.xlsx')); % Excel File Name
%Store Data in Excel Spreadsheet
xlswrite(xlName,strcat({'Average Snowball Radius in ['},scaleUnit,{']'}),'Sheet1','A1');
xlswrite(xlName,avgSnowballRadius,'Sheet1','A2');
xlswrite(xlName,{'Total Number of Snowballs'},'Sheet1','B1');
xlswrite(xlName,totalSnowballs,'Sheet1','B2');
xlswrite(xlName,strcat({'Snowball Size (a_i) in ['},scaleUnit,{']'}),'Sheet1','A4');
xlswrite(xlName,transpose(ai),'Sheet1','A5:A19');
xlswrite(xlName,{'Number of Snowballs (N_i)'},'Sheet1','B4');
xlswrite(xlName,transpose(N),'Sheet1','B5:B19');
clear;
```

## **APPENDIX D** – MATLAB CODE FOR 3D MICROSCOPE DISTRIBUTION BINNING

```
clear;
folder = 'Spreadsheets/'; % Spreadsheet Folder
scaleUnit = 'um'; % Units
titleName = input('Enter Excel file name: ', 's');
fileName = strcat(folder,titleName,'.xlsx');
dataIn = xlsread(fileName);
histogramImage = figure; % Open New Figure Window
hist(dataIn, 15); % Display histogram of snowball sizes in 15 bins
histTitle = strrep(titleName,'_','.'); % Format Histogram Title
title(textwrap(strcat('Snowball Distribution for',{' '},histTitle),30)); % Histogram Title
xlabel(strcat('Snowball Radius (a_i) in [',scaleUnit,'])); % Histogram X-axis Label
ylabel('Number of Snowballs (N)'); % Histogram Y-axis Label
[N, ai] = hist(dataIn, 15); % Store snowball distribution
totalSnowballs = sum(N); % Total number of snowballs
avgSnowballRadius = mean(dataIn); % Average size of snowballs
saveas(histogramImage,char(strcat('Results/',titleName,{' '},'- Histogram')),'png'); % Save
Histogram Image
close(histogramImage);
xlName = char(strcat('Results/',titleName,{' '},'- Data','.xlsx')); % Excel File Name
```

```
%Store Data in Excel Spreadsheet
xlswrite(xlName,strcat({'Average Snowball Radius in ['},scaleUnit,{']'}),'Sheet1','A1');
xlswrite(xlName,avgSnowballRadius,'Sheet1','A2');
xlswrite(xlName,{'Total Number of Snowballs'},'Sheet1','B1');
xlswrite(xlName,totalSnowballs,'Sheet1','B2');
xlswrite(xlName,strcat({'Snowball Size (a_i) in ['},scaleUnit,{']'}),'Sheet1','A4');
xlswrite(xlName,transpose(ai),'Sheet1','A5:A19');
xlswrite(xlName,{'Number of Snowballs (N_i)'},'Sheet1','B4');
xlswrite(xlName,transpose(N),'Sheet1','B5:B19');
clear;
```

## APPENDIX E – MATLAB CODE FOR AVERAGE DISTRIBUTION BINNING

```
clear;
folder = 'Spreadsheets/'; % Spreadsheet Folder
scaleUnit = 'um'; % Units
titleName = input('Enter Excel file name: ', 's');
fileName = strcat(folder,titleName,'.xlsx');
xMin = xlsread(fileName,'A1:A1');
xMax = xlsread(fileName,'A15:A15');
xSpan = xMax - xMin;
xInterval = xSpan/14;
xData = [xMin,0,0,0,0,0,0,0,0,0,0,0,0,0,xMax];
for i=2:14
   xData(i)=xMin + ((i-1)*xInterval);
end
xData = transpose(xData);
yData = xlsread(fileName,'B:B');
barImage = figure; % Open New Figure Window
bar(xData, yData, 1); % Display histogram of snowball sizes
histTitle = strrep(titleName,'_','.'); % Format Histogram Title
title(textwrap(strcat('Snowball Distribution for',{' '},histTitle),30)); % Histogram Title
```

```
xlabel(strcat('Snowball Radius (a_i) in [',scaleUnit,'])); % Histogram X-axis Label
ylabel('Number of Snowballs (N)'); % Histogram Y-axis Label
saveas(barImage,char(strcat('Results/',titleName,{' '},'- Histogram')),'png'); % Save
Histogram Image
close(barImage);
clear;
```

## APPENDIX F – PYTHON CODE FOR COMPOSITE SIMPSON'S RULE

```
def arcLengthSinX(mag=1, upper=math.pi, lower=0, n=10):
        '''mag   int      [int]            upper   float    [radians]
        lower   float    [radians]              n       int      [int]'''
        deltaX = (upper-lower)/n
        sumTotal = 0
        sumLoop = 0
        for i in range(n+1):
                xN = lower + (i*deltaX)
                if (i == 0) | (i == n):
                        sumLoop =
math.sqrt(1+(math.pow(mag,2)*math.pow(math.cos(xN),2)))
                elif i%2 != 0:
                        sumLoop =
4*math.sqrt(1+(math.pow(mag,2)*math.pow(math.cos(xN),2)))
                else:
                        sumLoop =
2*math.sqrt(1+(math.pow(mag,2)*math.pow(math.cos(xN),2)))
                sumTotal = sumTotal + sumLoop
        return round((deltaX/3)*sumTotal,4)
```

```
def arcLengthX2(mag=1, upper=1, lower=0, n=10):
        '''mag   int      [int]            upper   float    [radians]
        lower   float    [radians]              n       int      [int]    '''
        deltaX = (upper-lower)/n
        sumTotal = 0
        sumLoop = 0
        for i in range(n+1):
                xN = lower + (i*deltaX)
                if (i == 0) | (i == n):
                        sumLoop = math.sqrt(1+(4*math.pow(mag,2)*math.pow(xN,2)))
                elif i%2 != 0:
                        sumLoop =
4*math.sqrt(1+(4*math.pow(mag,2)*math.pow(xN,2)))
                else:
                        sumLoop =
2*math.sqrt(1+(4*math.pow(mag,2)*math.pow(xN,2)))
                sumTotal = sumTotal + sumLoop
        return round((deltaX/3)*sumTotal,4)
```

## APPENDIX G – DERIVATION OF EDDY CURRENT EQUATION

If: $\nabla \times \overrightarrow{H_S} = \overrightarrow{J_S}$

Then the on both sides is: $\nabla(\nabla \cdot \overrightarrow{H_S}) - \nabla^2 \overrightarrow{H_S} = \nabla \times \overrightarrow{J_S}$

From Gauss's law $\nabla \cdot \vec{H} = 0$, so: $-\nabla^2 \overrightarrow{H_S} = \nabla \times \overrightarrow{J_S}$

From Ohm's law $\vec{J} = \sigma \vec{E}$, so: $-\nabla^2 \overrightarrow{H_S} = \sigma \nabla \times \overrightarrow{E_S}$

From Faraday's law $\nabla \times \vec{E} = \frac{-\partial \vec{B}}{\partial t}$ so: $\nabla^2 \overrightarrow{H_S} = \sigma \frac{\partial \overrightarrow{B_S}}{\partial t}$

Finally, from [3]: $-\nabla^2 \overrightarrow{H_S} = -j\omega\mu\sigma \overrightarrow{H_S}$

So: $\sigma \nabla \times \overrightarrow{E_S} = -\nabla \times \overrightarrow{J_S} = -j\omega\mu\sigma \overrightarrow{H_S}$

As shown in (5).